[AMERICAN JOURNAL OF SCIENCE, VOL. 298, JANUARY, 1998, P. 1–29]

American Journal of Science

JANUARY 1998

GROWTH OF MINERAL ZONES BY DIFFUSION-CONTROLLED REACTIONS: THEORY AND APPLICATION TO MESOSIDERITES

ALEX RUZICKA*

Department of Planetary Sciences,
University of Arizona, Tucson, Arizona 85721

ABSTRACT. The theory of Fisher (1973, 1977) and Joesten (1977) for the steady-state growth of mineral zones by diffusion-controlled reactions is modified to explicitly and formally account for polymineralic reactants, open-system diffusive fluxes, and diffusion geometry. The modifications are illustrated by applying the theory to olivine coronas in mesosiderite meteorites.

Reactant composition strongly influences the growth of mineral zones and is embodied in the layer-growth model presented here by so-called "residual-concentration-effect" terms or "R-terms." The open-system modification is similar to that developed by Ashworth and Birdi (1990), and the effect of diffusion geometry is handled by the introduction of a simple geometrical factor. Using the new formalism, this paper presents quantitative criteria for the stable growth of quasi-steady-state zone structures (Frantz and Mao, 1975) and analytic expressions for zone widths, zone modes, and the relative change in chemical potential of any locally buffered component in a mineral zone within a stable zone structure. It is shown that if one or both of the initial reactants are polymineralic, then it is possible for a mineral to disappear by reaction in one part of the zone sequence and to reappear by reaction in another part, and for a mineral to be stable to diffusion within a layer structure even though it is removed by the overall structure-forming reaction.

The zone sequence, relative zone widths, and zone modes of olivine coronas in mesosiderites can be explained largely by layer growth models in which coupled reaction and diffusion occur between olivine and a polymineralic, mesosiderite-like matrix assemblage. A 5-component, closed-system model is adequate to explain many features of coronas, and a 7-component, open-system model yields similar results to the 5-component model when open-system fluxes are small. Some constraints on Onsager diffusion (L-) coefficient ratios, reactions, and the magnitude of open-system fluxes appropriate to corona growth in mesosiderites can be obtained, but uncertainties in the values for open-system fluxes make it difficult to place tight constraints on L-coefficient ratios, and *vice-versa*. For the Emery mesosiderite, it appears that P and Cr diffused into the coronas from a large volume of matrix, and that Fe diffused out of the coronas and into a large volume of matrix, during open-system diffusion. The combined effect of local reactions within coronas in Emery was to remove olivine, tridymite, plagioclase, metal, and clinopyroxene and to produce orthopyroxene, chromite, and merrillite. Most likely, metal was largely transferred from coronas to matrix by diffusional processes, and oxygen was supplied to coronas from the matrix.

SYMBOLS

J_i = diffusion flux of component i (mol/cm^2-s)
$J_i^{q'}$ = diffusive flux of component i adjacent to and away from qth reaction site
$J_i^{\rightarrow q}$ = diffusive flux of component i adjacent to and towards qth reaction site
τ = time (s)

* Present address: Planetary Geosciences Institute, Department of Geological Sciences, University of Tennessee, Knoxville, Tennessee 37996-1410.

μ_i = chemical potential of component i (cal/mol)
N_i^ϕ = formula proportion of component i in mineral phase ϕ (dimensionless)
N_i^r = stoichiometric coefficient of component in reaction r (dimensionless)
L_{ij} = Onsager coefficient for diffusion (mol²/cal-cm-s) of component i in response to the chemical potential gradient of component j; in the corona models, L_{ij} coefficients refer to oxides where i = MgO, $AlO_{3/2}$, etc. (abbreviated L_{MgMg}, L_{AlAl}, etc.)
α^q = effective cross-sectional area of qth reaction site, normal to diffusive flow (cm^2)
υ_i^q = an exchange cycle or reaction coefficient describing the addition (>0) or removal (<0) rate of component i by reaction at qth zone contact (mol/s); in the corona models, υ_i^q coefficients refer to oxides where i = MgO, $AlO_{3/2}$, etc. (abbreviated υ_{Mg}^q, υ_{Al}^q, etc.)
υ_ϕ^q = an exchange cycle or reaction coefficient describing the formation (>0) or removal (<0) rate of phase ϕ by direct reaction at qth zone contact (mol/s)
v^q = velocity of the qth zone contact (cm/s)
V_ϕ = molar volume of phase ϕ (cm^3/mol)
w^{zone} = absolute width of a mineral zone (cm)
W^{zone} = growth rate of a mineral zone (cm/s)
n_ϕ^{zone} = net production rate of mineral phase ϕ in a mineral zone (mol/cm^2-s)
R_ϕ^q = "residual-concentration-effect" term describing the rate at which mineral ϕ is transferred to an adjacent zone by the removal of the disappearing phase at the qth zone contact (mol/s)
P_ϕ^q = effective production rate of mineral phase ϕ at the qth zone contact (mol/s)
ϕd = a disappearing phase at the zone contact in question (mineral ϕ is present on only one side of contact and has $\upsilon_\phi^q < 0$); used as a subscript for υ and R
ϕc = a common phase at the zone contact in question (mineral ϕ is present on both sides of the contact in question and has either $\upsilon_\phi^q > 0$ or $\upsilon_\phi^q < 0$), or any other phase that has $\upsilon_\phi^q > 0$ at the contact in question; used as a subscript for υ and R
l = for a given zone, refers to a leading zone contact (the contact further away from the initial contact); used as a superscript for υ, R and α
t = for a given zone, refers to a trailing zone contact (the initial contact, or the contact closer to the initial contact); used as a superscript for υ, R and α
X_ϕ^{zone} = mole fraction of mineral ϕ in a mineral zone (dimensionless)
χ_ϕ^{zone} = volume fraction of mineral ϕ in a mineral zone (dimensionless)
k = number of components present locally
p = number of mineral phases present locally
s = number of reactions involving ith component
z = number of zone contacts where reactions are occurring

INTRODUCTION

Diffusion- and reaction-produced mineral zones such as coronas represent structures that formed during metamorphism (by diffusion metasomatism) in response to gradients in chemical potentials and afford a unique opportunity to study reaction and diffusion processes. This is because both the reactants and products of the reactions are (at least in part) preserved and because the details of the layer structures (zone sequences, zone modes, zone widths) can be sensitive to the diffusive fluxes involved in their formation. Thus, studies of layer-growth structures potentially allow reaction processes and mass-flux conditions during metamorphism to be reconstructed in detail.

During metamorphism, reaction rates should generally exceed diffusion rates for all but the very smallest structures, implying that local equilibrium will prevail during most metamorphic processes (Fisher and Elliot, 1974; Fisher, 1977, 1978; Fisher and Lasaga, 1981). If local equilibrium is maintained, then the chemical potential (μ) of one or more components is buffered by the local mineral assemblage, and μ-gradients within the

diffusion medium will be constrained by the composition of the locally co-existing crystalline phases (Korzhinskii, 1959; Joesten, 1977, 1991; Brady, 1977). Diffusion and reaction between thermodynamically incompatible reactants will produce mineral zone structures (Korzhinskii 1959, 1971; Thompson, 1959) that may evolve rapidly so as to attain quasi-steady-state diffusion fluxes, and quasi-steady stoichiometries of reactions at zone contacts (Fisher, 1973, 1977; Fisher and Lasaga, 1981). In a quasi-steady-state, the complete set of reaction stoichiometries at zone contacts defines the "exchange cycle." The exchange cycle can be used to determine the layering configuration and the modes and widths of the layers in the structure. For any particular structure involving quasi-steady-state growth and local equilibrium, the exchange cycle can be determined by simultaneously solving a set of local mass balance, steady flux, and local equilibrium equations if the ratios of Onsager diffusion coefficients (L-coefficients) of the diffusing components are known or are assumed (Fisher, 1973, 1977; Joesten, 1977, 1986a; Fisher and Lasaga, 1981; Ashworth and Birdi, 1990; Johnson and Carlson, 1990; see also Weare and others, 1976; Frantz and Mao, 1975, 1976, 1979; and Foster 1981, 1983, 1986, 1991 for similar approaches).

In this paper, the models developed by Fisher (1973, 1977) and Joesten (1977) are modified so as to facilitate their use for a larger variety of mineralogically zoned structures. The principal modification involves the way reactant composition is treated. It has long been recognized that reactant modal composition has an important influence on the development of mineral zone structures (Joesten, 1977; Foster, 1981, 1983, 1986, 1991; Swapp, 1988), but analytical expressions that quantify the effect for the general case have not (until now) been developed. In this paper, so-called "R-terms," which embody the effect of reactant modal composition, are incorporated into equations that are used to calculate the growth rates of phases and mineral zones. With this approach, polymineralic reactants can be modelled with the same equations that are used for monomineralic reactants. Another modification involves open-system fluxes. In his model, Joesten (1977) considered closed-system diffusion only. Open-system diffusion, with diffusion occurring between layer assemblages and their surroundings, was later considered by Joesten (1986b), Ashworth and Birdi (1990), Johnson and Carlson (1990), and Carlson and Johnson (1991). The equations used here to model open-system diffusion are similar to those used by Ashworth and Birdi (1990), although they are used in a different manner. Ashworth and Birdi (1990) focussed on the "inverse" approach of attempting to constrain the magnitude of open-system fluxes from the details of corona assemblages, while in this paper the "forward" approach is used, which calculates the corona assemblage that develops for given values of open-system fluxes.

The theory is illustrated by applying it to olivine coronas, which separate largely monomineralic olivine clasts from a polymineralic silicate-phosphate-metallic matrix, in the Emery and Morristown mesosiderite meteorites (Ruzicka and others, 1994). Table 1 summarizes petrologic data for coronas in Emery and Morristown. The coronas can be subdivided into three zones (table 1): (1) the *inner zone,* adjacent to olivine, primarily contains orthopyroxene and chromite; (2) the *middle zone* is rich in orthopyroxene, plagioclase, and often merrillite; and (3) the *outer zone,* adjacent to a tridymite-bearing and often metal-rich matrix, is similar to the middle zone except that it contains clinopyroxene and less merrillite. In Morristown, the inner zone can be subdivided into an orthopyroxene + chromite subzone immediately adjacent to olivine and into an orthopyroxene subzone adjacent to the middle zone.

The coronas in mesosiderites provide a striking example of coupled reaction-diffusion processes during high-temperature (850°–1200°C), anhydrous metamorphism (Powell, 1971; Floran, 1978; Nehru and others, 1980; Ruzicka and others, 1994). There is abundant evidence to suggest that local equilibrium was largely maintained during

TABLE 1

A. Petrologic data for olivine coronas and adjacent matrix in Emery (Ruzicka and others, 1994). Zone modes and widths refer to the relatively flat portions of the coronas. Coronas in Emery are 600 to 1000 μm thick and surround mm-sized olivine mineral clasts

Zone	ol	Inner	Middle	Outer	Matrix
Fractional width of corona	–	0.12–0.26	0.23–0.35	0.40–0.55	–
Mode (vol%)					
ol	100	0	0	0	0
opx	0	80–90	60	50–60	25–30
chr	trace	6–15	1–3	≤2	≤2
merr	0	2–6	6–15	7–11	2–3
plag	0	<1	20–25	20–30	20
cpx	0	<0.5	<0.1	<5	<5
ilm	0	1–2	1	≤2	≤2
troi	0	<0.5	≤0.2	≤1	≤2
kam	0	0	≤1	≤2	30–35
tae	0	≤0.2	0.1	≤2	5
trid	0	0	0	0	≤5

Phases:
ol = olivine; Fa_{27-41} mol percent (uniform for a given clast).
opx = orthopyroxene; $En_{73-63}Fs_{24-33}Wo_{2.1-3.8}$ mol percent.
chr = chromite; atomic Cr/(Cr + Al) ~ 0.75 to 0.85, Fe/(Fe + Mg) ~ 0.87 to 0.91, 2Ti/(2Ti + Cr + Al) ~ 0.05 to 0.10 typical, up to 0.25 in the inner zone of coronas.
merr = merrillite; essentially $Ca_3(PO_4)_2$ with 3.5 to 3.7 wt percent MgO, 0.8 to 1.0 wt percent FeO, 0.9 to 1.0 wt percent Na_2O.
plag = plagioclase; $An_{96-87}Or_{0-0.3}$ mol percent.
cpx = clinopyroxene; $En_{45-43}Fs_{15-17}Wo_{43-39}$ mol percent.
ilm = ilmenite.
troi = troilite.
kam = kamacite; ~93 wt percent Fe, ~7 wt percent Ni, ≤ 0.03 wt percent P, ≤ 0.01 wt percent Cr.
tae = taenite; mainly tetrataenite with ~51 wt percent Ni, ~49 wt percent Fe, ≤ 0.04 wt percent P, ≤ 0.03 wt percent Cr.
trid = tridymite; nearly pure SiO_2.

B. Petrologic data for olivine coronas and adjacent matrix in Morristown (Ruzicka and others, 1994). Zone modes and widths refer to the relatively flat portions of the coronas. Coronas in Morristown are between 300 to 400 μm thick and surround mm-sized olivine mineral and lithic clasts

Zone	ol	Inner*	Middle	Outer	Matrix
Fractional width of corona	–	0.12–0.22	0.19–0.25	0.57–0.68	–
Mode (vol%)					
ol	100	0	0	0	0
opx	0	86–92	50–65	65–70	60
chr	trace	6–12	≤2	≤0.5	1
merr	0	<2	≤3	≤1	1
plag	0	≤0.2	30–45	20–30	25–30
cpx	0	<0.1	<0.1	≤5	5
ilm	0	≤1	≤0.1	≤0.1	<1
troi	0	≤0.1	≤0.1	≤0.1	≤0.1
kam	0	0	0	≤0.1	≤0.1
tae	0	0	≤0.1	≤0.1	≤0.1
trid	0	0	0	0	5

Phases:
ol = olivine; Fa_{17-37} mol percent (uniform for given clast).
opx = orthopyroxene; $En_{82-67}Fs_{16-30}Wo_{1.2-2.3}$ mol percent.
cpx = clinopyroxene; $En_{47-49}Fs_{8-9}Wo_{43-44}$ mol percent.
Other abbreviations as in (A).
* Can be subdivided into a largely bimineralic opx + chr subzone (fractional width of corona ~0.05 to 0.11) adjacent to ol and into a monomineralic opx subzone (fractional width of corona ~0.06 to 0.12) adjacent to the middle zone.

metamorphic growth of the coronas, and that they primarily formed by diffusion-controlled processes (Nehru and others, 1980; Ruzicka and others, 1994). The bulk compositions of the coronas resemble a mixture of olivine and mesosiderite matrix, except that $PO_{5/2}$ and $CrO_{3/2}$ are enriched, and metallic Fe and total Fe are depleted in the coronas (Ruzicka and others, 1994).

MODELS FOR OLIVINE CORONAS IN MESOSIDERITES

In this paper, two specific growth models for olivine coronas in mesosiderites have been considered. Both models envision reaction and diffusion occurring between semi-infinite halfspaces of monomineralic olivine and a polymineralic matrix. The halfspace approximation is appropriate for modelling the relatively flat portions of coronas. In both models, oxygen is assumed to be a dependent component, always combining with cations to form MgO, $AlO_{3/2}$, CaO, SiO_2, TiO_2, $CrO_{3/2}$, and FeO. The two models, which are refered to as the "5-component model" and the "7-component model" throughout this paper, are summarized in table 2, along with the assumed compositions of mineral phases.

The 5-component model (MgO-$AlO_{3/2}$-CaO-SiO_2-$PO_{5/2}$) entails the reaction of forsterite (F) with a matrix containing enstatite (E), diopside (D), tridymite (T), anorthite (A), and merrillite (M) to form a corona assemblage during closed-system diffusion. It is assumed that $MgAl_2O_4$ spinel (S) is absent in the initial reactants but that it can form in the corona by reaction between forsterite and anorthite, dependent on the rate at which MgO and $AlO_{3/2}$ are supplied by diffusion. The proportions of enstatite, diopside, anorthite, tridymite, and merrillite in matrix are assumed to be equivalent to that of orthopyroxene, clinopyroxene, plagioclase, tridymite, and merrillite in average mesosiderite matrix (Delaney and others, 1981), respectively, although for reasons explained later, in many cases the abundance of merrillite in matrix was increased relative to that of the other phases.

The 7-component model (MgO-$AlO_{3/2}$-CaO-SiO_2-$PO_{5/2}$- $CrO_{3/2}$-FeO) entails the reaction of olivine (F) with a matrix containing orthopyroxene (E), chromite (S), merrillite (M), anorthite (A), clinopyroxene (D), kamacite (K), and tridymite (T). Closed-system diffusion for MgO, $AlO_{3/2}$, CaO, and SiO_2 is assumed, and because the coronas in mesosiderites cannot be regarded as mixtures of olivine and matrix for P, Cr, and Fe (see above), either closed- or open-system diffusion for $PO_{5/2}$, $CrO_{3/2}$, and FeO is assumed. The compositions and proportions of the phases in the matrix are assumed to be similar to those in the matrix of Emery (Ruzicka and others, 1994). The composition assumed for kamacite in the model (99.03 wt percent Fe, 0.65 wt percent P, 0.32 wt percent Cr) is representative of that inferred for Emery metal prior to corona formation and has slightly elevated contents of P and Cr compared to that currently found in Emery ($\leq$0.04 wt percent P and $\leq$0.03 wt percent Cr) (Ruzicka and others, 1994). However, nearly identical model results are obtained if kamacite is assumed to be pure Fe.

CONCEPTUAL FRAMEWORK

Before discussing the calculation procedure used to model layer growth, it is necessary to discuss briefly some of the concepts upon which the models rest. Of particular importance are the reference frame for diffusion and the kinds of layer structures that can form during quasi-steady-state diffusion.

Reference Frame and the Initial Contact

The reference frame used here is the inert marker frame (Hartley and Crank, 1949; Brady, 1975; Fisher, 1977). It is convenient to cast equations in terms of an inert marker

TABLE 2

The 5- and 7-component models described in this paper. 5-component model: *forsterite reacts with matrix; system is closed to all components (MgO, $AlO_{3/2}$, CaO, SiO_2, and $PO_{5/2}$); spinel can form by reaction between forsterite and anorthite.* 7-component model: *olivine reacts with matrix; system is closed to MgO, $AlO_{3/2}$, CaO, and SiO_2 and is either open or closed to $PO_{5/2}$, $CrO_{3/2}$, and FeO*

5-Component Model			7-Component Model		
Phase and Symbol	Composition (atomic)	Matrix Mode* (vol%)	Phase and Symbol	Composition** (atomic)	Matrix Mode** (vol%)
Forsterite (F)	Mg_2SiO_4	0	Olivine (F)	$(Mg_{0.62}Fe_{0.38})_2SiO_4$	0
Enstatite (E)	$MgSiO_3$	57.4	Orthopyroxene (E)	$Mg_{0.65}Fe_{0.32}Ca_{0.03}SiO_3$	28
Spinel (S)	$MgAl_2O_4$	0	Cr-spinel (S)	$Mg_{0.1}Fe_{0.9}Cr_{1.6}Al_{0.4}O_4$	1.5
Merrillite (M)	$Ca_3(PO_4)_2$	2.4	Merrillite (M)	$Ca_3(PO_4)_2$	2.5
Anorthite (A)	$CaAl_2Si_2O_8$	28.8	Anorthite (A)	$CaAl_2Si_2O_8$	21
Diopside (D)	$Ca_{0.5}Mg_{0.5}SiO_3$	3.3	Clinopyroxene (D)	$Ca_{0.43}Mg_{0.45}Fe_{0.12}SiO_3$	4
Tridymite (T)	SiO_2	8.1	Tridymite (T)	SiO_2	4
			Metal (K)	$Fe_{0.9846}P_{0.0117}Cr_{0.0037}$	39

* Average mode of matrix in mesosiderites normalized to 100 percent (Delaney and others, 1981).
** Representative phase compositions and matrix mode in Emery (Table 1a; Ruzicka and others, 1994).

that corresponds to the position of the "initial contact" between two reacting assemblages. For bi-directional growth of mineral zones, where two initial reactants are present, the initial contact will always occur *within* a mineral layer, although under some conditions it may be very close to, and hence practically indistinguishable from, a mineralogical zone boundary. Assuming that reactions occur primarily at layer contacts, the mineral zone containing the initial contact will be either (a) monomineralic, or (2) polymineralic and bimodal, with a discontinuity in mode (but not mineral assemblage) marking the location in bimodal layers (Joesten, 1977). In an inert marker frame, layer contacts separating different mineral assemblages will appear to move, but the initial contact will be stationary.

Quasi-steady-state Zone Sequences

The layer-forming process is initiated when reversible reaction occurs between two thermodynamically incompatible media. After the onset of appreciable diffusion, reactions will no longer be reversible, and irreversible growth of the zone structure will occur. Eventually, a quasi-steady-state condition will be obtained, in which zone modes and relative zone widths remain constant with time, even as the zones continue to widen. This section qualitatively discusses some of the conditions that must be met for zone structures to be stable to quasi-steady-state diffusion and defines terminology that is used to describe such structures.

For quasi-steady-state growth to occur, all zone contacts on the same side of the initial contact must move in one direction, and all zone contacts on the other side of the initial contact must move in the opposite direction. *For a given zone, the "leading contact" of the zone is the one farther from the initial contact, and the "trailing contact" of the zone is the one closer to the initial contact.* The leading contact will be the first to sweep past a given inert marker, with the trailing contact for the same zone passing the same inert marker at some later time. The initial contact itself can be regarded as the (stationary) "trailing" contact of the two modally distinct, but mineralogically identical, portions of the zones on either side of it.

Examples of possible quasi-steady-state, 5-component model olivine coronas in mesosiderites (see table 2 for mineral abbreviations) include:

F|ESM|EAM|EDAM|EDTAM (sequence **A**)

F|ES|EM|EAM|EDAM|EDTAM (sequence **B**)

F|ES|EM|EDM|EDAM|EDTAM (sequence **C**)

F|ES|EM|EDM|EAM|ETAM|EDTAM (sequence **D**)

in which zones are designated by the phases they contain (for example, the EAM zone contains enstatite, anorthite, and merrillite), and in which arrows above zone contacts indicate the sense of motion of the contacts in an inert marker frame. For sequence **A**, the initial contact between F and EDTAM occurs within the ESM zone, whereas for sequences **B**, **C**, and **D**, it occurs within the EM zone.

Four criteria must be met for a mineral zone sequence to be stable to diffusion-controlled reactions in a quasi-steady-state:

Criterion 1.–Local equilibrium must be maintained everywhere in the system, and thus the layer sequence must be consistent with phase equilibrium, mineral facies, or μ-diagrams (Korzhinskii, 1959, 1971; Joesten, 1977; Brady, 1977; Frantz and Mao, 1975). In other words, all phases that are in direct contact with one another (such as all the phases within a given zone or all the phases at a given zone contact) must coexist stably.

Criterion 2.–A particular phase assemblage cannot occur at more than one zone contact, for this would imply that chemical potentials were the same at multiple contacts, and thus that no μ-gradients were present between these contacts to drive diffusion. As can be readily verified, a different phase assemblage occurs at each zone contact in sequences **A** through **D**.

Criterion 3.–At each layer contact, at least one mineral has a negative growth rate and is being consumed by reaction, so that it appears only on one side of the contact. A phase that is being removed by reaction and appears only on one side of a given zone contact can be referred to conveniently as a "*disappearing phase*" (or "singular phase" in the terminology of Frantz and Mao, 1975) at the contact at which it disappears. Similarly, a phase that is being produced by reaction and that appears only on one side of a layer contact can be referred to as a "*newly-appearing*" phase at that contact. Finally, a phase that is present on both sides of a contact, and which can have either a positive or negative growth rate, can be referred to as a "*common phase*" at this contact (Frantz and Mao, 1975). Frantz and Mao (1975) showed that each layer contact will move in the direction of the zone containing a disappearing phase for that contact. This means that in an inert marker frame, all layer contacts will appear to move away from that layer in the zone structure that has the fewest number of minerals, and away from the initial interface between the reactants that bound the layer structure. For example, in the model zone sequence F|ESM|EAM|EDAM|EDTAM (sequence **A**), disappearing phases obviously include T at the EDAM-EDTAM contact and D at the EAM-EDAM contact, as these are the only phases that appear on only one side of the contacts. F must be the disappearing phase at the F-ESM contact if the corona is to grow bidirectionally. At the ESM-EAM contact, S must be a newly-appearing phase and A the disappearing phase, because S does not appear among the initial reactants. The initial interface between F and EDTAM will occur within the ESM layer.

Criterion 4.—For each modally distinct zone, the velocity of the leading contact must exceed the velocity of the trailing contact (Joesten, 1977, p. 661), for otherwise the zone will disappear with time. Thus, in an inert marker frame in which the initial contact is stationary, the zone contacts furthest from the initial contact will have the highest velocities and the zone contacts closest to the initial contact will have the lowest velocities.

CALCULATION PROCEDURE

Two basic calculation steps are involved in the quantitative modelling of steady-state growth of mineral zones by diffusion-controlled reactions. The first step is to determine the exchange cycle by simultaneously solving a set of mass balance and flux equations. The equations used in the exchange cycle calculation are similar to those outlined by Joesten (1977) but differ in detail. The second step is to incorporate the effect of reactant composition on layer growth. These steps are described below.

EXCHANGE CYCLE CALCULATION

To model the growth of mineral zones in diffusion/reaction structures, one needs to know the reaction rates for all components (υ_i) and mineral phases (υ_ϕ) at the reaction sites in the structure. The exchange cycle describes all reactions occurring in the system. Assuming that a quasi-steady-state flux has been achieved and that reactions occur at zone contacts, the exchange cycle generally may be calculated by solving the following three sets of equations simultaneously (see Ruzicka, ms, for more details):

$$\upsilon_i^q = -\sum_{\phi=1}^{p} N_i^\phi \upsilon_\phi^q \tag{1}$$

$$\sum_{i=1}^{k} N_i^\phi \frac{L_{SiSi}}{L_{ii}} \left(\sum_{m=1}^{q} \frac{\upsilon_i^m}{\alpha^m} + J_i^{\rightarrow 1} \right) = 0 \tag{2}$$

$$J_i^{\rightarrow 1} - J_i^{z\rightarrow} + \sum_{q=1}^{z} \frac{\upsilon_i^q}{\alpha^q} = 0 \tag{3}$$

where υ_i^q = addition (>0) or removal (<0) rate of component i from the diffusion medium at the qth contact; υ_ϕ^q = formation (>0) or dissolution (<0) rate of mineral phase ϕ by reaction at the qth contact; N_i^ϕ = formula proportion of component i in mineral phase ϕ; L_{SiSi}/L_{ii} is the ratio of a reference L-coefficient (for example, L_{SiSi}) to another L-coefficient (L_{ii}); α^q = effective reaction area parallel to diffusive flow at the qth contact; and $J_i^{\rightarrow 1}$ and $J_i^{z\rightarrow}$ represent steady fluxes of component i within the initial reactants. L-coefficients are generalized mobilities (Katchalsky and Curran, 1967) or diffusivities and measure the ease with which components are transported down gradients in chemical potentials (Brady, 1977). As written, (2) assumes that $L_{ij} = 0$ for $i \neq j$, although similar expressions could be written for situations in which this condition is not satisfied.

Eqs (1), (2), and (3) are similar to those used by Joesten (1977) to determine the exchange cycle, except that they have been modified to take into account various layer geometries (through the α term), and the possibility of open-system fluxes (through the $J_i^{\rightarrow 1}$ and $J_i^{z\rightarrow}$ terms). In this paper, the υ_i^q and υ_ϕ^q represent reaction rates, although per unit time they are equivalent to reaction stoichiometries, in the same sense as used by Joesten (1977).

In a growing quasi-steady-state zone structure, zones thicken and μ-gradients within each zone decrease, resulting in diminished *changes* in μ-gradients and consequently in diminished reaction rates at zone contacts (Fisher, 1977, p. 394). In this paper, one of the unknown reaction rates at a zone contact (for example, $\upsilon_{SiO_2}^{\text{corona-matrix}}$) is arbitrarily

specified, and all other results are scaled to this rate. Thus, the models describe the layer structure that forms in a quasi-steady-state at a particular moment in time, when $\upsilon_{SiO_2}^{corona\text{-}matrix}$ corresponds to a certain value.

When the number of equations, given by (1), (2), (3) and the arbitrary specification of a reaction rate, equal the number of unknowns (one reaction rate for each phase and component at each contact), the exchange cycle can be solved. However, in some circumstances, additional equations besides those given by (1), (2), and (3) are needed to calculate the exchange cycle.

For example, it can be shown that the exchange cycle for any spinel-bearing zone sequence in the 5-component model (table 2) cannot be determined without the use of an additional equation constraining the formation rate of spinel. In the 5-component model, $MgAl_2O_4$ spinel is absent in the initial reactants, and it can only form after layer growth has been initiated. For this model, it is assumed that spinel can form only as rapidly as MgO and $AlO_{3/2}$ are supplied to potential spinel-forming regions by the breakdown of forsterite and anorthite. Thus, the total rate of $MgAl_2O_4$ spinel formation by reaction (n_s^{rxn}, in mol/unit time-area) is expressed as:

$$n_S^{rxn} = \frac{1}{\alpha^{F\text{-}A}} \cdot minimum\ of\left(\upsilon_{MgO}^{F\text{-}A},\ 0.5\upsilon_{AlO_{3/2}}^{F\text{-}A}\right) \tag{4}$$

where $\upsilon_{MgO_{3/2}}^{F\text{-}A}$ and $\upsilon_{AlO_{3/2}}^{F\text{-}A}$ represent the respective rates of reaction of MgO and $AlO_{3/2}$ at any contacts located between forsterite and anorthite in a layer structure, and $\alpha^{F\text{-}A}$ represents the effective reaction area normal to diffusion in the spinel-forming region. Exchange cycle results for a spinel-free zone sequence are used to calculate n_S^{rxn} for an analogous spinel-bearing zone sequence. For example, the exchange cycle results for the zone sequence F|EAM|EDAM|EDTAM are used to calculate n_S^{rxn} for any sequence that contains one or more spinel-bearing layers between F and the partial structure . . . EAM|EDAM|EDTAM ($n_s \cdot \alpha = \min\left[\upsilon_{MgO}^{F\text{-}EAM},\ 0.5\upsilon_{AlO_{3/2}}^{F\text{-}EAM}\right]$). Although the total rate of spinel formation is constrained by (4), spinel in all other respects is treated the same way as other phases when solving the exchange cycle. In effect, this approach assumes that the 5-component model coronas will pass through a transient quasi-steady-state in which spinel is absent initially and then into a different transient quasi-steady-state in which spinel is present. The concept of multiple transient quasi-steady-states was also considered by Johnson and Carlson (1990) and Ashworth and coworkers (1992).

For the zone sequence F|ES|EM|EDM|EAM|ETAM|EDTAM (sequence **D**), yet an additional equation must be included in the exchange cycle calculation. This arises because diopside disappears by reaction at the ETAM-EDTAM contact but reappears by reaction at the EDM-EAM contact, a complication that can arise for certain combinations of L-ratios and reactant compositions. For sequence **D**, diopside initially present within matrix must ultimately reappear somewhere within the corona, unless it is removed by reaction, owing to mass balance constraints. In a sense, diopside is *transferred* from the matrix to the corona ($n_D^{transfer}$) until it reaches a zone in which it is stable to quasi-steady-state diffusion. (Such mass transfers are produced by a "residual-concentration-effect" and are described in more detail below.) The transfer rate of diopside is the same for any spinel-free layer sequence assuming the same L-coefficients, initial reactant composition, et cetera, and thus the exchange cycle results for any spinel-free layer assemblage can be used to constrain the transfer rate for diopside. Thus, for example,

$$\left(n_D^{transfer}\right)_{F|ES|EM|EDM|EAM|ETAM|EDTAM} = \left(n_D\right)_{F|EDAM|EDTAM} \tag{5}$$

where the second term (the molar amount of diopside formed in the EDAM layer per unit time per unit area normal to diffusive flow) can be readily calculated from the

exchange cycle results for F|EDAM|EDTAM. Although the rate of diopside transfer for sequence D is constrained by (5), diopside in all other respects is treated the same way as other phases when solving the exchange cycle.

To perform the exchange cycle calculation one must specify L-ratios in (2), any open-system fluxes within the initial reactants (J_i^{-1} and J_i^{z-}) in (2) and (3), the compositions of minerals (N_i^{ϕ}) in (1) and (2), and the effective reaction areas (α^q) in (2), (3), and (4). The effective reaction areas depend on the diffusion geometry assumed. For plane-parallel layers (as assumed here), α^q = constant, whereas for spherical geometry, $\alpha^q = 4\pi(r^q)^2$, where r^q = radius of the qth contact. In this paper, it was assumed that mineral compositions (N_i^{ϕ}) are constant throughout the system of interest.

INCORPORATING THE EFFECT OF REACTANT COMPOSITION

Residual-Concentration-Effect

For layer sequences composed of monomineralic layers and reactants, the effective growth rates of phases are given directly by the exchange cycle coefficients. However, for polymineralic layers and reactants, the effective growth rates of phases depend not only on the direct reaction rates, given by the exchange cycle, but also on the modal compositions of the reactants.

A simple example illustrates the difference between a system with mono- and polymineralic reactants. If the matrix of mesosiderites consisted of tridymite alone, the coronas could be modelled as follows:

$$\leftarrow \quad \rightarrow$$
$$\mathrm{F|E|T}$$

where E = enstatite growing by reaction at the expense of forsterite (F) and tridymite (T). For closed-system diffusion, the effective growth (or production) rates of E at the F-E and E-T contacts, $P_E^{F\text{-}E}$ and $P_E^{E\text{-}T}$, respectively, are given by:

$$P_E^{F\text{-}E} = \frac{v_E^{F\text{-}E}}{\alpha^{F\text{-}E}}, \qquad P_E^{E\text{-}T} = \frac{v_E^{E\text{-}T}}{\alpha^{E\text{-}T}}, \tag{6A}$$

and the velocities of the layer contacts are given by:

$$v^{F\text{-}E} = -v_E^{F\text{-}E}\left[\frac{V_E}{\alpha^{F\text{-}E}}\right], \qquad v^{E\text{-}T} = v_E^{E\text{-}T}\left[\frac{V_E}{\alpha^{E\text{-}T}}\right] \tag{6B}$$

where V_E = molar volume of enstatite, and where velocities away from F are arbitrarily taken to be positive. In mesosiderites, the matrix is rich in orthopyroxene, and a better representation of the coronas is given by:

$$\leftarrow \quad \rightarrow$$
$$\mathrm{F|E|ET.}$$

Assuming that L-coefficients (as well as mineral compositions and open-system fluxes) are the same for F|E|T as for F|E|ET, the exchange cycle coefficients of phases in F|E|T will be the same as in F|E|ET. Moreover, the effective growth rates for F and E at the F-E contact and the velocity of the F-E contact will be the same for F|E|T as for F|E|ET. However, the presence of some E in the ET zone will cause the velocity of the E-ET contact to be greater than the velocity of the E-T contact. This arises because there is less T to be removed from a bimineralic ET reactant, than there is T to be removed from a monomineralic reactant, for a given removal rate of T. Thus, the E-ET layer contact will move more rapidly than the E-T layer contact. Similarly, the effective

production rate of E at the E-ET contact will be greater than the effective production rate of E at the E-T contact, because the removal of T at E-ET causes E to be concentrated in a residue that is added to the E zone. The latter effect, which can be regarded as a transfer of E from ET to E by the removal of T, is here referred to as the "residual-concentration-effect." This rate of transfer of E at the E-ET contact, $R_E^{E\text{-}ET}$, is given by mass balance:

$$R_E^{E\text{-}ET} = -\upsilon_T^{E\text{-}ET}\left(\frac{X_E^{ET}}{X_T^{ET}}\right) \tag{7}$$

where $\upsilon_T^{E\text{-}ET}$ = reaction rate of the disappearing phase (tridymite) at the E-ET contact, X_T^{ET} = mole fraction of tridymite in the reactant, and X_E^{ET} = the mole fraction of enstatite in the reactant. The effective production rate of E at the E-ET contact, $P_E^{E\text{-}ET}$, can be found from:

$$P_E^{E\text{-}ET} = \frac{\upsilon_E^{E\text{-}ET} + R_E^{E\text{-}ET}}{\alpha^{E\text{-}ET}} \tag{8A}$$

and the velocity of the E-ET contact is now:

$$v^{E\text{-}ET} = [\upsilon_E^{E\text{-}ET} + R_E^{E\text{-}ET}]\left[\frac{V_E}{\alpha^{E\text{-}ET}}\right] \tag{8B}$$

In (7), as $X_E^{ET} \rightarrow 0$ (and as $X_T^{ET} \rightarrow 1$), $R_E^{E\text{-}ET} \rightarrow 0$, and the F|E|ET corona increasingly resembles that of F|E|T (as needs be the case). Conversely, as $X_E^{ET} \rightarrow 1$ (and as $X_T^{ET} \rightarrow 0$), $R_E^{E\text{-}ET} \rightarrow \infty$, and the effective production rate of E at E-ET (given by (8A)) and the velocity of the E-ET contact (given by (8B)) become infinitely large.

This example demonstrates the importance of the residual-concentration-effect, which must be considered for any mineral zone that grows at the expense of a polymineralic reactant. The existence of a residual-concentration-effect follows from criterion 3 for quasi-stable zone growth. As the zone contact of a polymineralic reactant sweeps past a given inert marker, at least one mineral (a disappearing phase) in the reactant must be completely removed by reaction, which will result in a concentration of all the non-disappearing (that is, common) phases in the reactant. The importance of the residual-concentration-effect for assessing zone sequence stability as well as for determining zones modes and widths was previously recognized by Joesten (1977; see his eq 10-12) and by Swapp (1988), but neither of these authors generalized the concept.

The mass-transfer rate at which phases are concentrated in the "residue" produced by the removal of a disappearing phase is given by a so-called R-term:

$$R_\phi^q = -\upsilon_{\phi d}^q\left(\frac{X_\phi}{X_{\phi d}}\right)^* \tag{9}$$

where $\upsilon_{\phi d}^q$ = the exchange cycle reaction rate of the disappearing phase at the qth contact, $X_{\phi d}$ = the mole fraction of the disappearing phase in the reactant, and X_ϕ = the mole fraction of any phase in the same reactant. The "*" and hence the mole fraction ratio in (9) refer to the reactant zone from which the disappearing phase is being removed. If ϕ happens to be a disappearing phase ($\phi = \phi d$), then application of (9) yields:

$$R_{\phi=\phi_d}^q = -\upsilon_{\phi d}^q\left(\frac{X_{\phi=\phi d}}{X_{\phi d}}\right)^* = -\upsilon_{\phi d}^q, \tag{10}$$

and the R-term has a negative value equal to the loss rate of the disappearing phase at the contact at which it is disappearing. Eq (9) is applicable to any zone contact in any

quasi-steady-state zone sequence in which all reactions are modelled as occurring at zone contacts and is consistent with the method that Joesten (1977) used to determine zone modes and widths.

Zone Modes and Thicknesses

As shown in the previous section, R_ϕ can be regarded as a *production* term for mineral ϕ at a leading contact of a mineral zone. If the effective production rates, given by equations analogous to (8A), of all phases at a layer contact are known, then the mode of the layer can be calculated. Mineral proportions within a given zone are determined by reactions at the leading contact of a growing layer, as the leading contact of any zone will move past a given inert marker before the trailing contact of the zone has had a chance to move past the marker. Thus, the molar fraction of mineral ϕ in a zone (X_ϕ^{zone}) and the volume fraction of mineral ϕ in a zone (χ_ϕ^{zone}) can be expressed as:

$$X_\phi^{zone} = \left[\frac{\upsilon_\phi^l + R_\phi^l}{\sum_{\phi=1}^{p} \upsilon_\phi^l + R_\phi^l}\right] \tag{11A}$$

$$\chi_\phi^{zone} = \left[\frac{(\upsilon_\phi^l + R_\phi^l)V_\phi}{\sum_{\phi=1}^{p} (\upsilon_\phi^l + R_\phi^l)V_\phi}\right] \tag{11B}$$

where the superscript l refers to the leading contact and where V_ϕ is the molar volume of mineral ϕ. (In this paper, the molar volumes of Robie and others, 1978, were used.)

In a layer structure experiencing quasi-steady-state growth, the thickness ratios of zones remain unchanged even though the absolute thicknesses of individual zones continue to increase with time. Unlike modes, the thickness of a mineral zone depends on reactions that occur both at the leading and trailing contacts of the zone (Joesten, 1977). The growth rate (W^{zone}) or width per unit time of a mineral zone is given by the difference in velocity between the leading and trailing contacts:

$$W^{zone} = \frac{w^{zone}}{\tau} = \left[\frac{1}{\sigma^l}\sum_{\phi=1}^{p} (\upsilon_\phi^l + R_\phi^l)\cdot V_\phi\right] - \left[\frac{1}{\alpha^t}\sum_{\phi=1}^{p} R_\phi^t \cdot V_\phi\right]. \tag{12}$$

If the trailing contact happens to correspond to the initial contact, then $R_\phi^t = 0$, and the second bracketed term in (12) equals zero.

In practice, the calculation of modal compositions and relative zone thicknesses for polymineralic reaction/diffusion zones proceeds one zone (for uni-directional growth) or two zones (for bi-directional growth) at a time, because the composition and width of any zone depends on the composition of the adjacent zone or initial reactant out of which the zone is forming. After the exchange cycle is determined, R-terms are calculated for the zone contacts immediately adjacent to the initial reactants by using (9). This enables the modes of the zones immediately adjacent to the initial reactants to be determined by using (11). This procedure is repeated for the next adjacent zone or zones (closer to the initial contact), and continued until the modes of all zones have been determined. Once modal compositions have been calculated for all zones, the relative widths of the zones can be determined by using (12).

Evaluating Zone Sequence Stability

The stability criteria for mineral zone sequences stable to quasi-steady-state diffusion, previously discussed qualitatively, can now be put into a quantitative form. If ϕd

represents a disappearing phase and ϕc any other phase at the qth contact, then criterion 3 for steady-state growth implies:

$$\upsilon^{q}_{\phi d} < 0 \tag{13A}$$

and

$$\upsilon^{q}_{\phi c} + R^{q}_{\phi c} \geq 0 \tag{13B}$$

whereas criterion 4 for steady-state growth implies:

$$n^{zone}_{\phi} = \left[\frac{\upsilon^{l}_{\phi} + R^{l}_{\phi}}{\alpha^{l}}\right] - \left[\frac{R^{l}_{\phi}}{\alpha^{l}}\right] \geq 0 \tag{13C}$$

While all diffusion-controlled zone sequences stable to quasi-steady-state diffusion must satisfy (13), not all zone sequences that meet these criteria may actually be achieved in real systems, because of constraints imposed on the fluxes of diffusing components by the stoichiometry of the minerals present (Joesten, 1977, p. 657) and by the composition of the initial reactants.

Influence of Initial Reactant Composition

Reactant composition during zone growth is an important variable in determining the sequence, widths, and compositions of zones that form by diffusion-controlled reactions. An increase in the modal abundance of a mineral in a reactant will tend to result in more of this mineral being present in the zones forming at the expense of this reactant and will tend to stabilize zone sequences in which the mineral appears in multiple mineral zones. Conversely, a decrease in the modal abundance of a mineral in a reactant will result in less of this mineral being present in the zones forming at the expense of this reactant and will tend to stabilize zone sequences in which the mineral appears in a small number of mineral zones.

Average mesosiderite matrix in the five-component model system (with molar $X_E^{EDTAM} = 0.7178$; $X_D^{EDTAM} = 0.0394$; $X_T^{EDTAM} = 0.1207$; $X_A^{EDTAM} = 0.1126$; $X_M^{EDTAM} = 0.0095$) is relatively poor in merrillite and diopside and rich in enstatite, tridymite, and anorthite (Delaney and others, 1981). Owing to their low abundances, the distribution of merrillite and diopside in the model coronas will depend greatly on the composition assumed for the matrix and on the assumed L-ratios. This is illustrated for merrillite by the L-ratio plots L_{PP}/L_{SiSi} versus L_{AlAl}/L_{SiSi} (fig. 1). Figure 1A shows the zone sequences that form if merrillite is always present in sufficient proportions in the matrix to prevent this mineral from becoming a disappearing phase, whereas figure 1B shows the zone sequences that develop for a fixed matrix merrillite/tridymite molar ratio of 0.10, similar to that in average mesosiderite matrix (0.08). As L_{PP}/L_{SiSi} is progressively increased, more merrillite tends to be removed by reaction close to matrix, and more tends to be produced by reaction away from matrix within the corona. For a given matrix composition, this will tend to result in zone sequences in which merrillite is absent in two or more zones either adjacent to matrix (sequences **E** and **F**) or in the central-to-outer portion of the coronas (sequences **G**, **H**, **I**, **J**) (fig. 1B). On the other hand, if the merrillite/tridymite ratio in the matrix is relatively high, merrillite will appear throughout larger portions of the coronas (fig. 1A). Merrillite is always concentrated immediately adjacent to the initial contact in an EM or ESM zone, both because of the residual-concentration-effect, and because local buffering by merrillite and other phases in 5-component model coronas tends to cause $PO_{5/2}$ to diffuse mainly toward olivine (as shown in fig. 2 and discussed below).

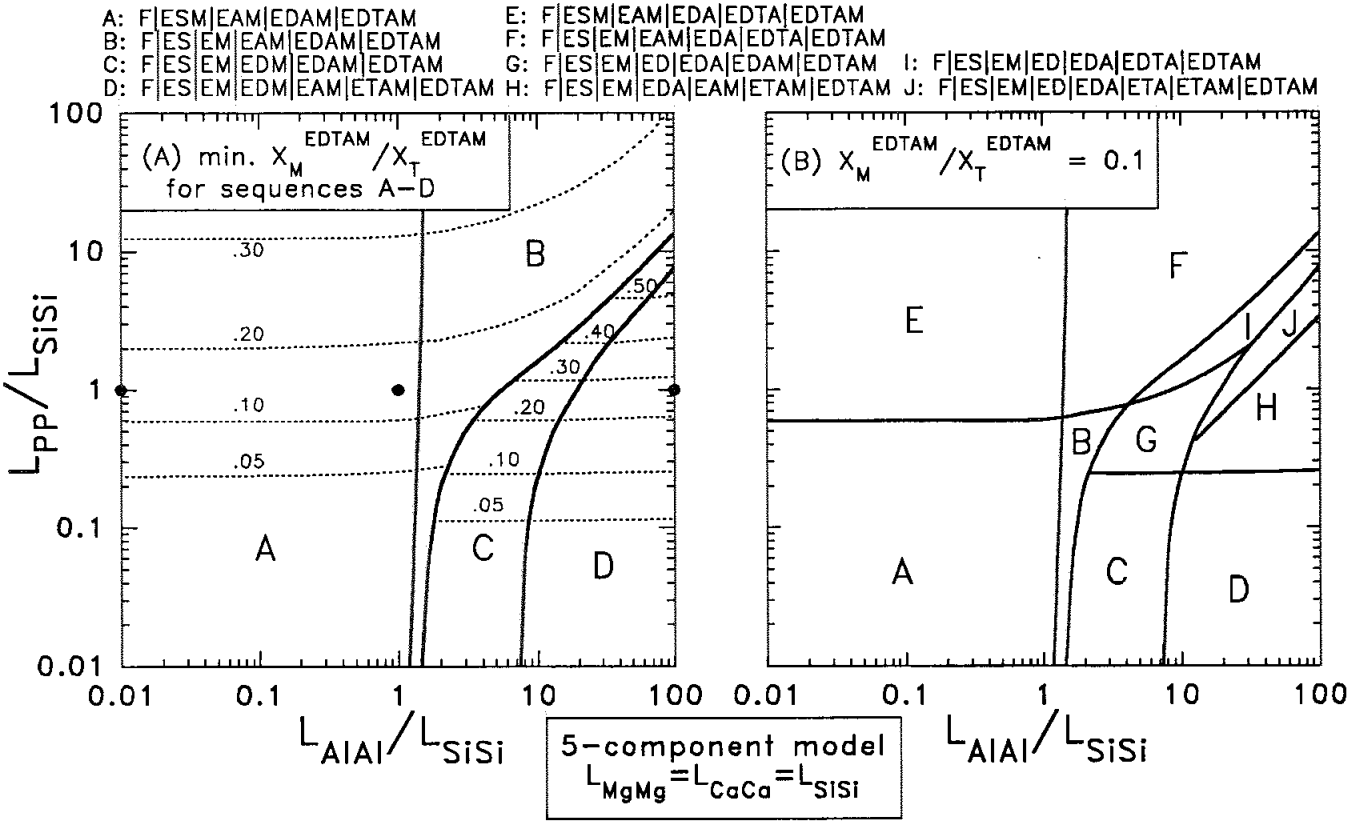

Fig. 1. L-ratio diagrams illustrating the effect of matrix (EDTAM) composition and L_{AlAl}/L_{SiSi} and L_{PP}/L_{SiSi} on the stability of various quasi-steady-state model corona zone sequences. The 5-component model was assumed; see table 2 for mineral abbreviations and other information regarding this model. All calculations assume that $L_{MgMg}/L_{SiSi} = L_{CaCa}/L_{SiSi} = 1$, and that the proportions of E, D, A, and T in EDTAM are similar to that of orthopyroxene, clinopyroxene, plagioclase, and tridymite, respectively, in average mesosiderite matrix (Delaney and others, 1981). **(A)** shows the minimum values of molar X_M^{EDTAM}/X_T^{EDTAM} (dotted lines) necessary to stabilize zone sequences **A, B, C,** and **D**, assuming a sufficient supply of matrix merrillite to prevent this mineral from becoming a *disappearing phase* in the coronas. Heavy lines delineate the stability limits of sequences **A, B, C,** and **D** under these conditions. Solid dots indicate the conditions examined in figure 2. **(B)** shows the stability limits (heavy lines) of various zone sequences when molar $X_M^{EDTAM}/X_T^{EDTAM} = 0.10$, which is representative of the merrillite/tridymite ratio in average mesosiderite matrix. Note the correspondence between the position of zone sequence transitions in (B) with the 0.10 contour in (A).

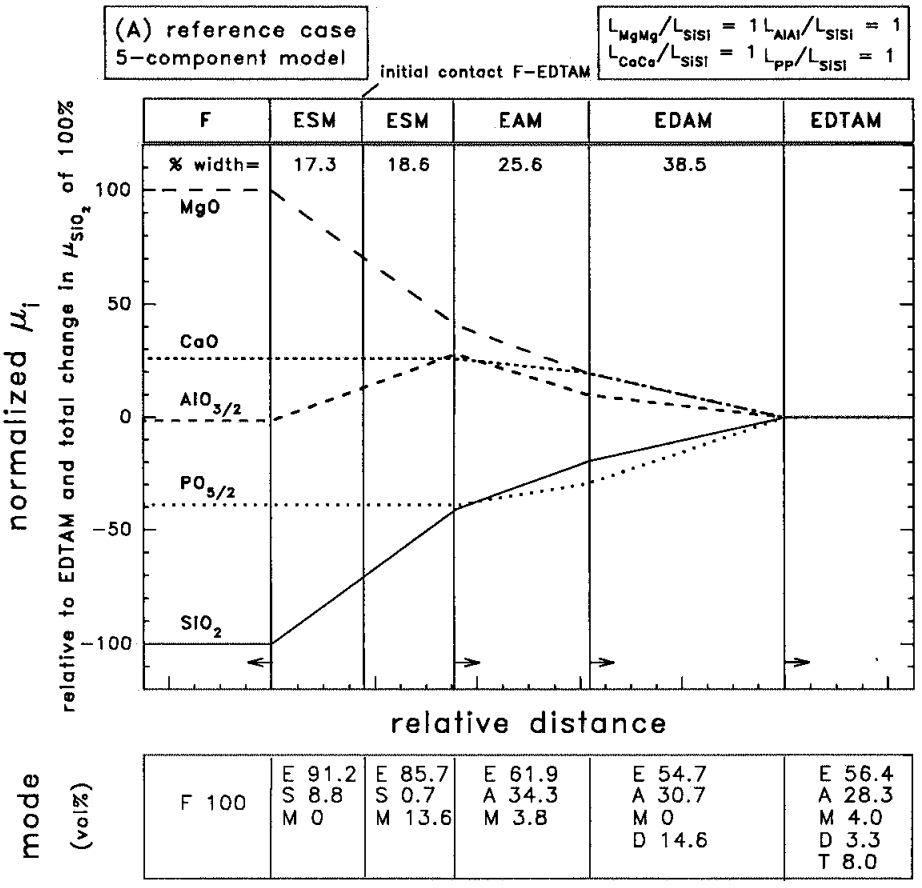

Fig. 2. Plots summarizing the zone sequences, relative zone widths, zone modal compositions, and relative chemical potential variations for three quasi-steady-state model coronas, produced with three different sets of L-ratios and matrix (EDTAM) compositions. The 5-component model was assumed; see table 2 for mineral abbreviations and other information regarding this model. Numbers near the top of the plots represent fractional zone widths (total corona width = 100), and arrows at zone contacts indicate the sense of motion of the contacts in an inert marker reference frame. Exchange cycle and net reaction coefficients for each of the three cases are given in table 3 (cases 1–3). (**A**) Reference case for a 5-component model corona produced when all L-coefficients equal one another, and when the merrillite (M) abundance in EDTAM has been increased relative to average mesosiderite matrix so as to just prevent M from becoming a *disappearing phase* at the EDAM-EDTAM contact. F |ESM |EAM |EDAM |EDTAM is the stable sequence. (**B**) 5-component model corona produced when L_{AlAl} is much smaller than other L-coefficients, and when the M abundance of EDTAM has been increased relative to average mesosiderite matrix so as to just prevent M from becoming a *disappearing phase* at the EDAM-EDTAM contact. F|ESM|EAM|EDAM|EDTAM is the stable sequence. (**C**) 5-component model corona produced when L_{AlAl} is much larger than other L-coefficients, and when the M abundance of EDTAM has been increased relative to average mesosiderite matrix so as to just prevent M from becoming a *disappearing phase* at the EDM-EAM contact. F |ES |EM |EDM |EAM |ETAM |EDTAM is the stable sequence.

The zone sequences in figure 1A and 1B differ greatly in their spatial distribution of diopside, suggesting that a change in the abundance of matrix diopside should affect the L-ratio space over which the zone sequences will be stable. From the previous discussion, one would predict that an increase in the abundance of matrix diopside should stabilize those zone sequences in which diopside appears in multiple corona zones. Indeed, calculations show that increasing the amount of matrix diopside will increase the stability range of sequence **C** relative to **B** and **D** and of **G** and **I** relative to sequences **F**, **J**, and **H** (fig. 1).

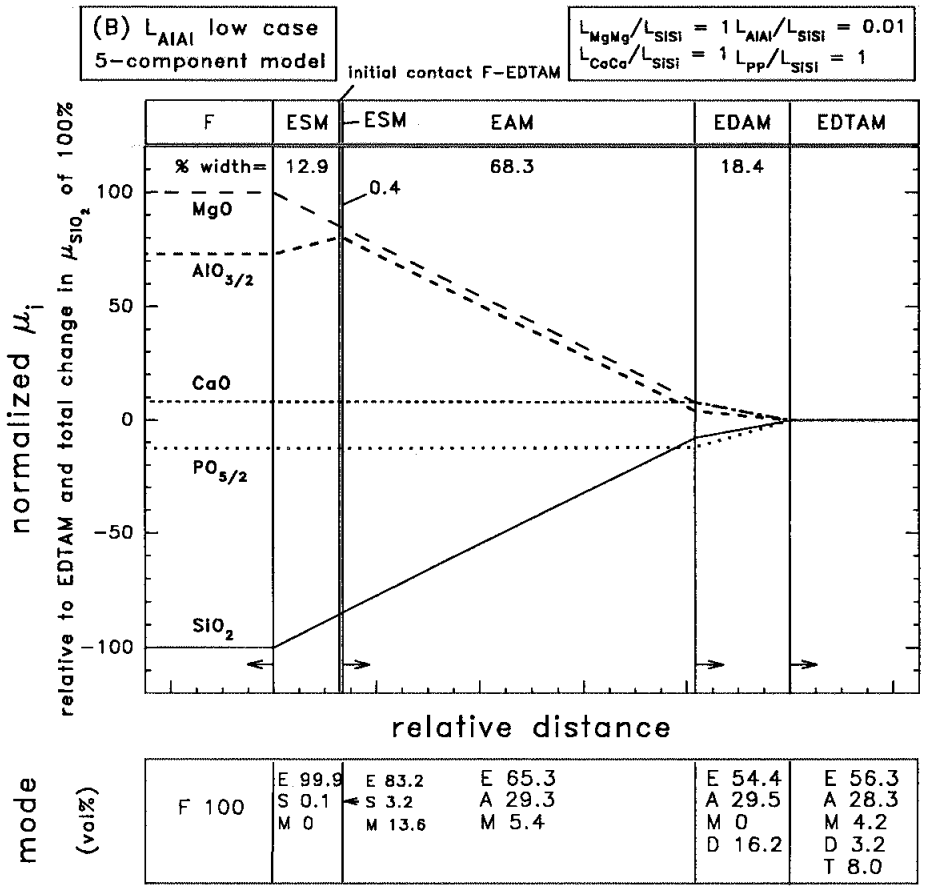

Fig. 2 (continued)

μ-VARIATIONS ACROSS MINERAL ZONES

The variation in chemical potentials across mineral zones and the change in chemical potential gradients across zone contacts can be determined for a quasi-steady-state zone sequence by combining knowledge of L-coefficients, reaction rates of components at zone contacts, diffusion geometry, open-system fluxes in the initial reactants (if any), and zone thicknesses. As chemical potential gradients are ultimately responsible for driving diffusion, an analysis of these gradients is useful for understanding why particular layer structures form and for predicting how changes in L-coefficients will affect layer structure growth.

Assuming for simplicity that $L_{ij} = 0$ for $i \neq j$ and that L_{ii} = constant, then:

$$J_i^{q\rightarrow} - J_i^{\rightarrow q} = -L_{ii}\nabla\mu_i^{q\rightarrow} + L_{ii}\nabla\mu_i^{\rightarrow q} = L_{ii}\Delta(\nabla\mu_i)^q = \frac{v_i^q}{\alpha^q} \pm J_i^{open} \tag{14A}$$

$$\Delta(\nabla\mu_i)^q = \frac{1}{\tau}\left[\frac{\Delta\mu_i^{\rightarrow q}}{W^{\rightarrow q}} - \frac{\Delta\mu_i^{q\rightarrow}}{W^{q\rightarrow}}\right] = \frac{v_i^q}{\alpha^q L_{ii}} \pm \frac{J_i^{open}}{L_{ii}} \tag{14B}$$

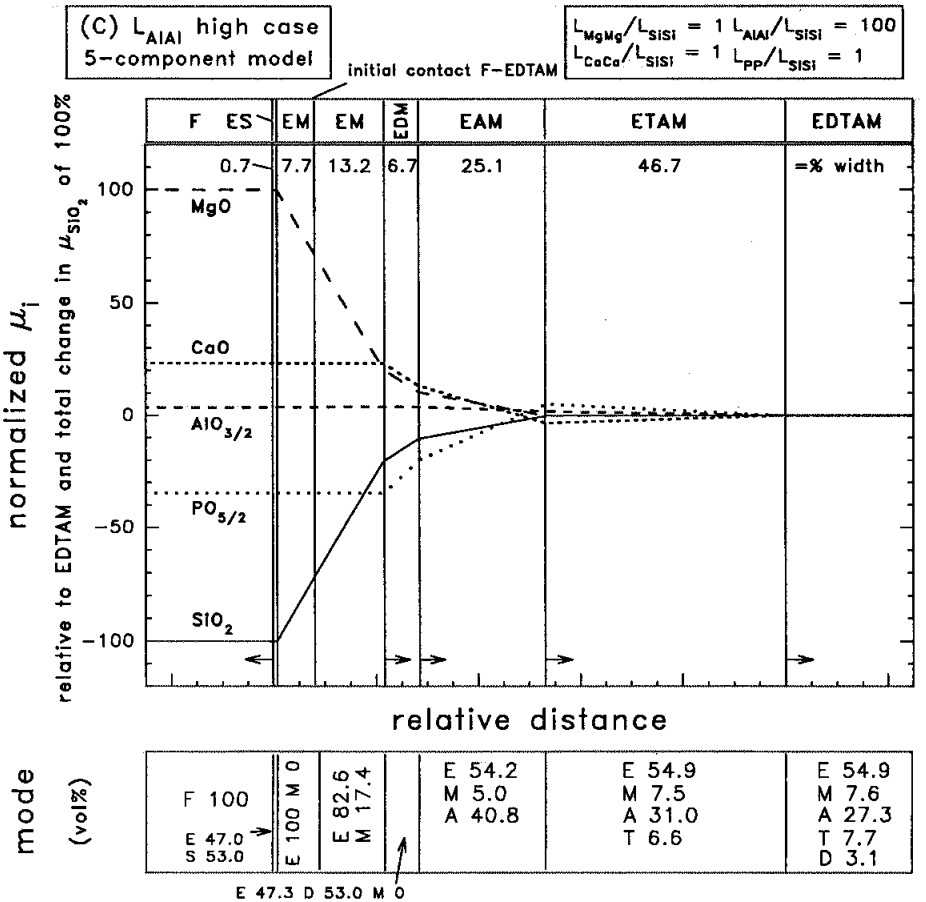

Fig. 2 (continued)

where $J_i^{\rightarrow q}$ = flux in the zone adjacent to and *toward* the qth contact; $J_i^{q\rightarrow}$ = flux in the zone adjacent to and *away* from the qth contact; J_i^{open} = open-system flux into or out of the corona; $\Delta[\nabla\mu_i]^q$ = the change in chemical potential gradient across the qth contact; υ_i^q = reaction rate of component i at the qth contact; α^q = effective reaction area normal to diffusive flow at the qth contact; $W^{zone}(=w^{zone}/\tau)$ = growth rate of a mineral zone; and τ = time elapsed. It should be noted if $L_{ij} \neq 0$ for $i \neq j$, then expressions similar to (14) can be written by replacing L_{ii} in (14) with an "effective binary" diffusion coefficient (S. Chakraborty, personal communication). (14B) can be rearranged to solve for the change in chemical potential within any given zone ($\Delta\mu_i^{\rightarrow q}$, $\Delta\mu_i^{q\rightarrow}$, or simply $\Delta\mu_i^{zone}$). To obtain absolute values for $\Delta\mu_i^{zone}$ from eq [14B], absolute values for all relevant parameters (L_{ii}, υ_i^q, α^q, and W) must be known. However, to obtain relative or time-invariant changes in $\Delta\mu_i^{zone}$, only relative values for these parameters are needed (L-ratios, relative υ_i^q, relative α^q, relative W). Alternatively, eq (14B) may be used to model absolute zone thicknesses (if $\Delta\mu_i^{zone}$, υ_i^q, α^q, τ, and L_{ii} are known or assumed) or to model the time elapsed in steady-state growth (if $\Delta\mu_i^{zone}$, υ_i^q, α^q, L_{ii}, and W are known or assumed).

As an example of eq (14), consider the 7-component model corona F|ES|ESM|ESMA|ESMAD|ESMADKT. For the 7-component model, it is assumed

that open-system fluxes within the ESMADKT initial reactant can be non-zero for some components, and that there are no open-system fluxes within F. Defining J_i^{out} as the open-system flux of i through ESMADKT away from the ESMAD-ESMADKT contact and out of the corona, eq (14B) leads to:

$$\frac{\Delta\mu_i^{ESMAD}}{\tau} = \left(\frac{\upsilon_i^{ESMAD\text{-}ESMADKT}}{\alpha^{ESMAD\text{-}ESMADKT}} - J_i^{out}\right)\left(\frac{W^{ESMAD}}{L_{ii}}\right) \quad (15A)$$

$$\frac{\Delta\mu_i^{ESMA}}{\tau} = \left(\frac{\upsilon_i^{ESMA\text{-}ESMAD}}{\alpha^{ESMA\text{-}ESMAD}} + \frac{\upsilon_i^{ESMAD\text{-}ESMADKT}}{\alpha^{ESMAD\text{-}ESMADKT}} - J_i^{out}\right)\left(\frac{W^{ESMAD}}{L_{ii}}\right) \quad (15B)$$

$$\frac{\Delta\mu_i^{ESM}}{\tau} = \left(\frac{\upsilon_i^{ESM\text{-}ESMA}}{\alpha^{ESM\text{-}ESMA}} + \frac{\upsilon_i^{ESMA\text{-}ESMAD}}{\alpha^{ESMA\text{-}ESMAD}} + \frac{\upsilon_i^{ESMAD\text{-}ESMADKT}}{\alpha^{ESMAD\text{-}ESMADKT}} - J_i^{out}\right)\left(\frac{W^{ESM}}{L_{ii}}\right) \quad (15C)$$

$$\frac{\Delta\mu_i^{ES(ESM)}}{\tau} = \left(\frac{\upsilon_i^{ES\text{-}ESM}}{\alpha^{ES\text{-}ESM}} + \frac{\upsilon_i^{ESM\text{-}ESMA}}{\alpha^{ESM\text{-}ESMA}} + \frac{\upsilon_i^{ESMA\text{-}ESMAD}}{\alpha^{ESMA\text{-}ESMAD}} + \frac{\upsilon_i^{ESMAD\text{-}ESMADKT}}{\alpha^{ESMAD\text{-}ESMADKT}} - J_i^{out}\right) \cdot \left(\frac{W^{ES(ESM)}}{L_{ii}}\right) \quad (15D)$$

$$\frac{\Delta\mu_i^{ES(F)}}{\tau} = \left(\frac{-\upsilon_i^{F\text{-}ES}}{\alpha^{F\text{-}ES}}\right)\left(\frac{W^{ES(F)}}{L_{ii}}\right) \quad (15E)$$

for all modally distinct zones within the corona, where the superscript ES(F) refers to that portion of the ES zone adjacent to F, the superscript ES(ESM) refers to that portion of the ES zone adjacent to the ESM zone, and $\Delta\mu_i^{zone}$ is measured from F to ESMADKT. For an open-system flux through ESMADKT *toward* the ESMAD-ESMADKT contact and into the corona, J_i^{out} (15) has a negative value (equal to positive J_i^{in}).

Examples of μ_i versus distance plots for model olivine coronas are shown in figure 2 (5-component model) and figure 3 (7-component model) and are discussed below. On all such plots, the values for $\Delta\mu_i$ within mineral zones depend on local buffering constraints (encapsulated in eq 2) and on L-ratios. Inflections in $\nabla\mu_i$ occur at all zone contacts that have a change in mineralogy, because of a difference in the buffering constraints on either side of the contacts. A *concave-downward inflection* in the gradient of μ_i corresponds to a region of local addition of i to the diffusion medium ($\upsilon_i^q > 0$) and by local mass balance constraints (eq 1), to a region where i-bearing minerals are being partially or completely removed by reaction. Conversely, a *concave-upward inflection* in the gradient of μ_i corresponds to a region of local removal of i from the diffusion medium ($\upsilon_i^q < 0$) and to a region where i-bearing minerals are being locally produced by reactions.

An overall decrease in μ_{SiO_2} from matrix to olivine is pre-supposed by assuming that SiO_2 is evolved at a contact adjacent to or close to the matrix. For example, for the 5-component model corona F|ESM|EAM|EDAM|EDTAM (fig. 2A,B), the parameter $\upsilon_{SiO_2}^{EDAM\text{-}EDTAM}$ was set to an arbitrary positive value (table 3, cases 1-2), corresponding to the release of SiO_2 by reaction into the diffusion medium at the EDAM-EDTAM contact. A similar assumption was made for the other model coronas (table 3, cases 3-5).

MODELLING RESULTS

5-Component Model Coronas–Three Examples

For the 5-component model, calculations reveal that the value of the diffusivity parameter L_{AlAl} has a large effect on layer growth. Consequently, model results for three five-component coronas with different values of L_{AlAl} are shown in figure 2 and in table 3.

For the "reference case" (fig. 2A; table 3, case 1), all L-coefficients have equal values, and the model corona F|ESM|EAM|EDAM|EDTAM is stable. For the "L_{AlAl}-low case" (fig. 2B; table 3, case 2), the value of L_{AlAl} is much smaller than for other L-coefficients, and the model corona F|ESM|EAM|EDAM|EDTAM is stable. Finally, for the "L_{AlAl}-high case" (fig. 2C; table 3, case 3), the value of L_{AlAl} is much larger than for other L-coefficients, and the model corona F|ES|EM|EDM| EAM|ETAM|EDTAM is stable. For each case, a matrix composition similar to that of average mesosiderite matrix has been assumed, except that the merrillite abundance was increased as necessary to just prevent merrillite from becoming a disappearing phase in the model coronas. This assumption was made because merrillite does not appear to have been a disappearing phase in coronas from Emery and Morristown.

If L_{AlAl} is relatively small, $AlO_{3/2}$ diffuses sluggishly, and the change in $\mu_{AlO_{3/2}}$ across coronas is relatively large (fig. 2b). Sluggish diffusion of $AlO_{3/2}$ results in negligible rates of reaction involving Al (υ^{q}_{Al}) (table 3, case 2), because little $AlO_{3/2}$ can be transported down gradients in $\mu_{AlO_{3/2}}$ to reaction sites. Consequently, the modal proportion of Al-bearing anorthite (A) in various zones (that grew in place of the EDTAM reactant) is relatively constant (fig. 2B).

In contrast, if L_{AlAl} is relatively large, the model corona F|ES|EM|EDM| EAM|ETAM|EDTAM is stable (fig. 2C). $AlO_{3/2}$ diffuses rapidly, and the change in $\mu_{AlO_{3/2}}$ across the model corona is very small (fig. 2C). Large expanses of Al-free mineral zones (EM and EDM) are produced within corona where $\mu_{AlO_{3/2}}$ is locally high (fig. 2C), because $AlO_{3/2}$ is transported rapidly away from areas where $\mu_{AlO_{3/2}}$ is high to areas where it is low. Reaction rates involving Al (υ^{q}_{Al}) are correspondingly large, and a large amount of Al-spinel is produced in the overall corona-forming reaction for this model corona (table 3, case 3).

A tridymite-bearing ETAM zone for the L_{AlAl}-high model corona is stable, because for this condition diopside (D) is consumed before tridymite (T) at the corona-matrix contact. Buffering by tridymite + enstatite in the ETAM zone results in $d\mu^{ETAM}_{SiO_2} = d\mu^{ETAM}_{MgO} = 0$, and thus SiO_2 and MgO are neither evolved nor consumed at the ETAM-EDTAM contact (fig. 2C). For this sequence, it was assumed that Si is evolved at the EAM-ETAM contact ($\upsilon^{EAM\text{-}ETAM}_{Si} > 0$), so that SiO_2 diffuses toward olivine. Tridymite is stable within the corona in the ETAM zone even though it is removed in the net corona-forming reaction (table 3, case 3). This demonstrates that *the mere appearance of a mineral in a layer within a quasi-steady-state zone sequence does not necessarily imply anything about whether the mineral was produced, removed, or left unchanged in the overall layer-forming process.*

Figure 2C also illustrates an interesting aspect of some model coronas, namely the disappearance of a given phase at one contact and the reappearance of the same phase at another contact. In fig. 2C, diopside disappears by reaction at the ETAM-EDTAM contact and reappears by reaction at the EDM-EAM contact. While this may seem counterintuitive, it does not violate any of the stability criteria for quasi-steady-state zone sequences. Different mineral assemblages are present at each zone contact, and at no two points between F and EDTAM within this model corona are the same values of μ_i for all components attained (fig. 2C). The stable existence of this zone sequence shows that for some combinations of L-ratios and reactant compositions, *a phase can disappear by reaction in one part of the corona and reappear by reaction in another part.* A somewhat similar conclusion was reached by Foster (1991) for mineral segregations in pelitic rocks.

5-Component Model–Correspondence to Actual Coronas

Calculations involving various L-ratios and matrix modes with the 5-component model suggest that reasonably good analogues to coronas in Emery and Morristown can

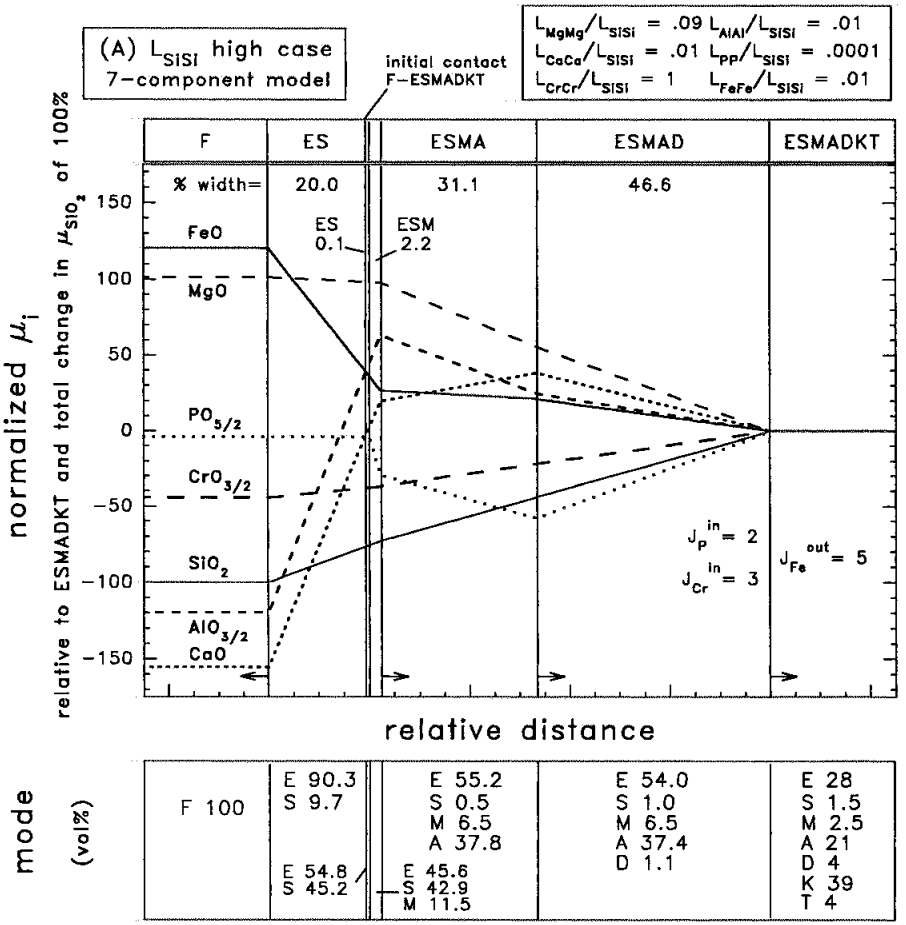

Fig. 3. Plots summarizing the zone sequences, relative zone widths, zone modal compositions, and relative chemical potential variations for two quasi-steady-state model coronas, produced with two different sets of L-ratios and open-system fluxes. The 7-component model was assumed; see table 2 for mineral abbreviations and other information regarding this model. Open-system fluxes of P and Cr into the corona (J_P^{in}, J_{Cr}^{in}) and Fe out of the corona (J_{Fe}^{out}) at the ESMAD-ESMADKT contact are expressed in terms of moles/(unit time-area), relative to $v_{Si}^{ESMAD\text{-}ESMADKT}$ = 12 moles/(unit time). Numbers near the top of the plots represent fractional zone widths (total corona width = 100), and arrows at zone contacts indicate the sense of motion of the contacts in an inert marker reference frame. Exchange cycle and net reaction coefficients for both cases are given in table 3 (cases 4 and 5). **(A)** Analog to Emery coronas produced when the value of L_{SiSi} is relatively high and the values for open-system fluxes are relatively small. F|ES|ESM|ESMA|ESMAD|ESMADKT is the stable sequence. The ES (adjacent F), ESMA, and ESMAD zones are analogous to the inner, middle, and outer zones of coronas in Emery, respectively; the narrow and spinel-rich ES (adjacent ESM) and ESM zones could correspond to the chromite-rich necklace often found at the inner-middle zone contact in such coronas. **(B)** Analog to Emery coronas produced when the value of L_{SiSi} is relatively small and the values of open-system fluxes are relatively large. F|ES|ESM|ESMA|ESMAD|ESMADKT is the stable zone sequence. The ES, ESMA, and ESMAD zones are analogous to the inner, middle, and outer zones of coronas in Emery, respectively; the M-rich, A-absent ESM zone could correspond to the merrillite-rich, plagioclase-depleted portion of the middle zone sometimes found immediately adjacent to the inner zone in such coronas.

be produced by coupled reaction and diffusion between forsterite and a silicate-phosphate assemblage but only if the abundance of merrillite is enhanced over that currently found in the matrix of the meteorites. Otherwise, merrillite tends to become a disappearing phase in the coronas, and one or more merrillite-free zones will develop between matrix and the initial olivine-matrix contact. As most of the P within mesosiderites

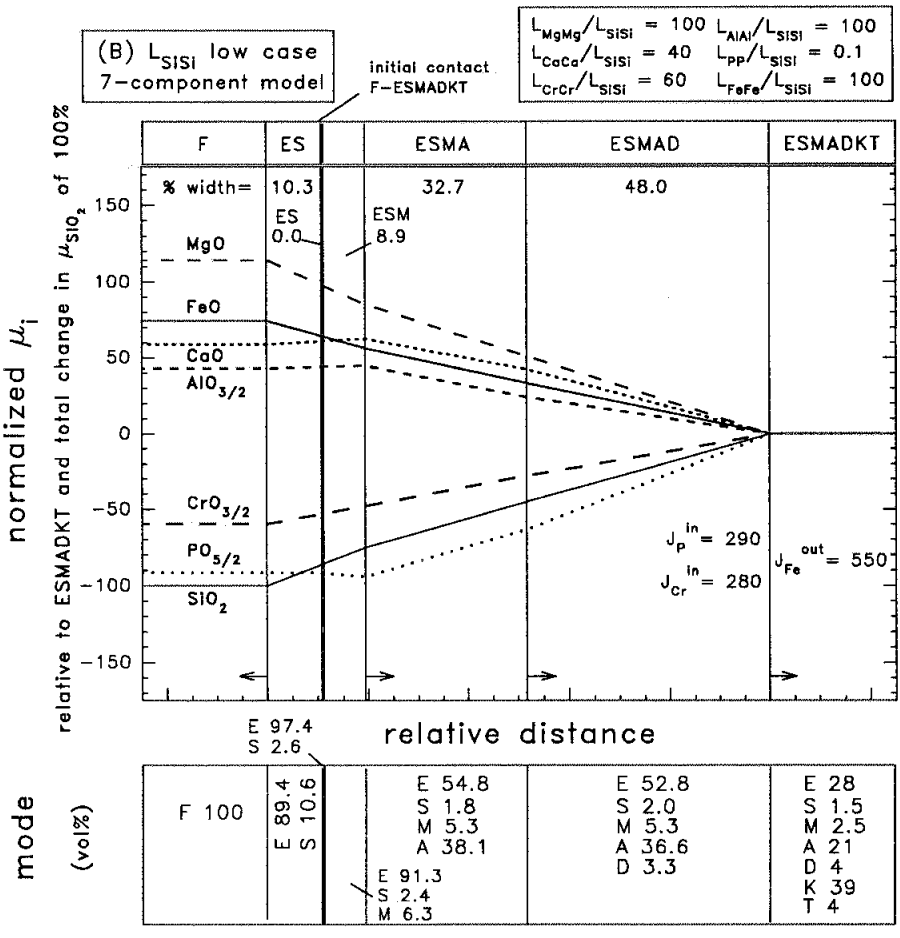

Fig. 3 (continued)

currently resides in merrillite, this suggests that the present P content of mesosiderite matrix is insufficient to account for the amount and distribution of merrillite within the coronas. The same conclusion can be reached from mass balance considerations (Ruzicka and others, 1994).

With the 5-component model, the model sequence F|ESM|EAM|EDAM|EDTAM provides the best analog to coronas in Emery, with the ESM, EAM, and EDAM zones in the model corresponding largely to the inner, middle, and outer zones of Emery coronas, respectively (table 1). In contrast, the model sequence F|ES|EM|EAM|EDAM|EDTAM provides the best analog to coronas in Morristown, with the ES and EM zones corresponding to the orthopyroxene + chromite and orthopyroxene subzones of the inner zone of Morristown coronas, respectively, and the EAM and EDAM zones corresponding to the middle and outer zones of Morristown coronas, respectively (table 1).

Assuming that merrillite is sufficiently abundant in the matrix to prevent it from becoming a disappearing phase, the best match between 5-component model and observed coronas for Morristown is obtained with $L_{SiSi} \approx 8$ $L_{AlAl} \approx 50$ $L_{MgMg} \approx 250$ to 1000 L_{PP}. For Emery, the best match is obtained when $L_{SiSi} > 3$ L_{CaCa} and when $L_{SiSi} \approx 3$

TABLE 3

Exchange cycle and net reaction coefficients for five selected cases of the 5- and 7-component models described in the text. Zone sequences for each of the cases are given in the table footnote

	5-Component Model			7-Component Model	
	Case 1	Case 2	Case 3	Case 4	Case 5
L-ratios:					
L_{MgMg}/L_{SiSi}	1	1	1	0.08	100
L_{AlAl}/L_{SiSi}	1	0.01	100	0.01	100
L_{CaCa}/L_{SiSi}	1	1	1	0.01	40
L_{PP}/L_{SiSi}	1	1	1	0.0001	0.1
L_{CrCr}/L_{SiSi}	–	–	–	1	60
L_{FeFe}/L_{SiSi}	–	–	–	0.01	100
Open-system flux (mol/unit-time-area):					
J_P^{in}	0	0	0	2	290
J_{Cr}^{in}	–	–	–	3	280
J_{Fe}^{out}	–	–	–	5	550
*Matrix mode (mol%).***					
E	71.28	71.23	70.19	12.84	12.84
S	0	0	0	0.5	0.5
M	1.63	1.71	3.15	0.37	0.37
A	11.18	11.17	11.01	3.01	3.01
D	3.91	3.91	3.85	1.75	1.75
K	0	0	0	79.36	79.36
T	11.99	11.98	11.80	2.18	2.18
Exchange cycle coefficients (mol/unit-time):					
$\upsilon_{Mg}^{F\text{-}ESM}$	38.63	31.63	$\upsilon_{Mg}^{F\text{-}ES}$ 8.58	$\upsilon_{Mg}^{F\text{-}ES}$ 0.17	1942.7
$\upsilon_{Al}^{F\text{-}ESM}$	−19.32	−0.16	$\upsilon_{Al}^{F\text{-}ES}$ −429.01	$\upsilon_{Al}^{F\text{-}ES}$ −1.04	−116.1
$\upsilon_{Ca}^{F\text{-}ESM}$	0	0	$\upsilon_{Si}^{F\text{-}ES}$ −8.58	$\upsilon_{Ca}^{F\text{-}ES}$ −1.00	−101.3
$\upsilon_{Si}^{F\text{-}ESM}$	−38.63	−31.63	$\upsilon_{P}^{F\text{-}ES}$ −231.67	$\upsilon_{Si}^{F\text{-}ES}$ −15.52	−16.4
$\upsilon_{P}^{F\text{-}ESM}$	0	0	$\upsilon_{E}^{F\text{-}ES}$ 240.25	$\upsilon_{Cr}^{F\text{-}ES}$ −4.17	−464.4
Exchange cycle coefficients (mol/unit-time):					
$\upsilon_{F}^{E\text{-}ESM}$	−86.93	−63.34	$\upsilon_{S}^{E\text{-}ES}$ 214.51	$\upsilon_{Fe}^{E\text{-}ES}$ 0.53	1211.9
$\upsilon_{E}^{E\text{-}ESM}$	125.56	94.98	$\upsilon_{Mg}^{ES\text{-}EM}$ 101.25	$\upsilon_{F}^{E\text{-}ES}$ −17.83	−3360.0
$\upsilon_{S}^{E\text{-}ESM}$	9.66	0.08	$\upsilon_{Al}^{ES\text{-}EM}$ 405.01	$\upsilon_{E}^{E\text{-}ES}$ 33.35	3376.4
$\upsilon_{M}^{E\text{-}ESM}$	0	0	$\upsilon_{Ca}^{ES\text{-}EM}$ 0	$\upsilon_{S}^{E\text{-}ES}$ 2.61	290.3
$\upsilon_{Mg}^{ESM\text{-}EAM}$	−19.16	−0.35	$\upsilon_{Si}^{ES\text{-}EM}$ −101.25	$\upsilon_{Mg}^{ES\text{-}ESM}$ −0.01	−0.0
$\upsilon_{Al}^{ESM\text{-}EAM}$	35.91	0.47	$\upsilon_{P}^{ES\text{-}EM}$ 0	$\upsilon_{Al}^{ES\text{-}ESM}$ 0.00	0.0
$\upsilon_{Ca}^{ESM\text{-}EAM}$	5.77	0.10	$\upsilon_{E}^{ES\text{-}EM}$ 101.25	$\upsilon_{Ca}^{ES\text{-}ESM}$ 0.02	0.6
$\upsilon_{Si}^{ESM\text{-}EAM}$	19.16	0.35	$\upsilon_{S}^{ES\text{-}EM}$ −202.51	$\upsilon_{Si}^{ES\text{-}ESM}$ −0.01	−0.0
$\upsilon_{P}^{ESM\text{-}EAM}$	−8.66	−0.14	$\upsilon_{M}^{ES\text{-}EM}$ 0	$\upsilon_{P}^{ES\text{-}ESM}$ 0.01	0.4
$\upsilon_{E}^{ESM\text{-}EAM}$	18.36	0.27	$\upsilon_{Mg}^{EM\text{-}EDM}$ −67.99	$\upsilon_{Cr}^{ES\text{-}ESM}$ 0.00	0.0
$\upsilon_{S}^{ESM\text{-}EAM}$	0.80	0.08	$\upsilon_{Ca}^{EM\text{-}EDM}$ 41.84	$\upsilon_{Fe}^{ES\text{-}ESM}$ −0.00	−0.0
$\upsilon_{M}^{ESM\text{-}EAM}$	4.33	0.07	$\upsilon_{Si}^{EM\text{-}EDM}$ 67.99	$\upsilon_{E}^{ES\text{-}ESM}$ 0.01	0.0
$\upsilon_{A}^{ESM\text{-}EAM}$	−18.76	−0.31	$\upsilon_{P}^{EM\text{-}EDM}$ −62.76	$\upsilon_{S}^{ES\text{-}ESM}$ −0.00	−0.0
$\upsilon_{Mg}^{EAM\text{-}EDAM}$	−7.47	−19.28	$\upsilon_{E}^{EM\text{-}EDM}$ 203.98	$\upsilon_{M}^{ES\text{-}ESM}$ −0.01	−0.2
$\upsilon_{Al}^{EAM\text{-}EDAM}$	−10.59	−0.25	$\upsilon_{M}^{EM\text{-}EDM}$ 31.38	$\upsilon_{Mg}^{ESM\text{-}ESMA}$ 1.22	−589.5
$\upsilon_{Ca}^{EAM\text{-}EDAM}$	6.23	11.90	$\upsilon_{A}^{EM\text{-}EDM}$ −271.97	$\upsilon_{Al}^{ESM\text{-}ESMA}$ 1.20	906.7
$\upsilon_{Si}^{EAM\text{-}EDAM}$	7.47	19.28	$\upsilon_{Mg}^{EDM\text{-}EAM}$ −29.84	$\upsilon_{Ca}^{ESM\text{-}ESMA}$ 0.90	425.5
$\upsilon_{P}^{EAM\text{-}EDAM}$	−9.34	−17.86	$\upsilon_{Al}^{EDM\text{-}EAM}$ 266.91	$\upsilon_{Si}^{ESM\text{-}ESMA}$ 3.79	4.5
$\upsilon_{E}^{EAM\text{-}EDAM}$	33.01	58.09	$\upsilon_{Ca}^{EDM\text{-}EAM}$ −22.70	$\upsilon_{P}^{ESM\text{-}ESMA}$ −0.01	−1.6
$\upsilon_{A}^{EAM\text{-}EDAM}$	5.29	0.13	$\upsilon_{Si}^{EDM\text{-}EAM}$ 29.84	$\upsilon_{Cr}^{ESM\text{-}ESMA}$ −2.09	−13.5
$\upsilon_{M}^{EAM\text{-}EDAM}$	4.67	8.93	$\upsilon_{P}^{EDM\text{-}EAM}$ 34.05	$\upsilon_{Fe}^{ESM\text{-}ESMA}$ −0.51	−297.4
$\upsilon_{D}^{EAM\text{-}EDAM}$	−51.07	−77.63	$\upsilon_{E}^{EDM\text{-}EAM}$ −177.39	$\upsilon_{E}^{ESM\text{-}ESMA}$ −2.07	905.6

to 5 $L_{MgMg} \approx 7$ to 10 $L_{AlAl} \approx 7$ to 20 L_{PP}. L_{CaCa} is poorly constrained for Emery as it depends greatly on the exact mode chosen for the matrix.

The *net* or *overall* structure-forming reaction in model coronas can be determined by summing all local reactions described by the exchange cycle. In the 5-component corona

TABLE 3
(continued)

	5-Component Model			7-Component Model	
	Case 1	Case 2	Case 3	Case 4	Case 5
$\upsilon_{Mg}^{EDAM\text{-}EDTAM}$	−12	−12	$\upsilon_{D}^{EDM\text{-}EAM}$ 414.46	$\upsilon_{S}^{ESM\text{-}ESMA}$ 1.31	8.5
$\upsilon_{Al}^{EDAM\text{-}EDTAM}$	−6	−0.06	$\upsilon_{M}^{EDM\text{-}EAM}$ −17.02	$\upsilon_{M}^{ESM\text{-}ESMA}$ 0.01	0.8
$\upsilon_{Ca}^{EDAM\text{-}EDTAM}$	−12	−12	$\upsilon_{A}^{EDM\text{-}EAM}$ −133.46	$\upsilon_{A}^{ESM\text{-}ESMA}$ −0.86	−455.0
$\upsilon_{Si}^{EDAM\text{-}EDTAM}$	12*	12*	$\upsilon_{Mg}^{EAM\text{-}ETAM}$ −12	$\upsilon_{Mg}^{ESMA\text{-}ESMAD}$ −0.17	6.0
Exchange cycle coefficients (mol/unit-time):					
$\upsilon_{P}^{EDAM\text{-}EDTAM}$	18	18	$\upsilon_{Al}^{EAM\text{-}ETAM}$ −138.05	$\upsilon_{Al}^{ESMA\text{-}ESMAD}$ −0.09	−151.4
$\upsilon_{E}^{EDAM\text{-}EDTAM}$	−24	−26.97	$\upsilon_{Ca}^{EAM\text{-}ETAM}$ −21.24	$\upsilon_{Ca}^{ESMA\text{-}ESMAD}$ 0.18	123.9
$\upsilon_{D}^{EDAM\text{-}EDTAM}$	72	77.94	$\upsilon_{Si}^{EAM\text{-}ETAM}$ 12*	$\upsilon_{Si}^{ESMA\text{-}ESMAD}$ −0.27	−0.0
$\upsilon_{A}^{EDAM\text{-}EDTAM}$	3	0.03	$\upsilon_{P}^{EAM\text{-}ETAM}$ 31.86	$\upsilon_{P}^{ESMA\text{-}ESMAD}$ −0.00	−0.5
$\upsilon_{M}^{EDAM\text{-}EDTAM}$	−9	−9	$\upsilon_{E}^{EAM\text{-}ETAM}$ 12	$\upsilon_{Cr}^{ESMA\text{-}ESMAD}$ 0.36	32.7
$\upsilon_{I}^{EDAM\text{-}EDTAM}$	−66	−63.03	$\upsilon_{A}^{EAM\text{-}ETAM}$ 69.03	$\upsilon_{Fe}^{ESMA\text{-}ESMAD}$ 0.04	−30.3
			$\upsilon_{M}^{EAM\text{-}ETAM}$ −15.93	$\upsilon_{E}^{ESMA\text{-}ESMAD}$ 0.78	339.4
			$\upsilon_{I}^{EAM\text{-}ETAM}$ −162.05	$\upsilon_{S}^{ESMA\text{-}ESMAD}$ −0.22	−20.5
			$\upsilon_{Mg}^{ETAM\text{-}EDTAM}$ 0	$\upsilon_{M}^{ESMA\text{-}ESMAD}$ 0.00	0.2
			$\upsilon_{Al}^{ETAM\text{-}EDTAM}$ −104.86	$\upsilon_{A}^{ESMA\text{-}ESMAD}$ 0.09	79.8
			$\upsilon_{Ca}^{ETAM\text{-}EDTAM}$ 2.10	$\upsilon_{D}^{ESMA\text{-}ESMAD}$ −0.69	−499.0
			$\upsilon_{Si}^{ETAM\text{-}EDTAM}$ 0	$\upsilon_{Mg}^{ESMAD\text{-}ESMADKT}$ −1.21	−1359.1
			$\upsilon_{P}^{ETAM\text{-}EDTAM}$ −3.15	$\upsilon_{Al}^{ESMAD\text{-}ESMADKT}$ −0.07	−639.2
			$\upsilon_{E}^{ETAM\text{-}EDTAM}$ 59.25	$\upsilon_{Ca}^{ESMAD\text{-}ESMADKT}$ −0.10	−448.7
			$\upsilon_{I}^{ETAM\text{-}EDTAM}$ −45.61	$\upsilon_{Si}^{ESMAD\text{-}ESMADKT}$ 12*	12*
			$\upsilon_{A}^{ETAM\text{-}EDTAM}$ 52.43	$\upsilon_{P}^{ESMAD\text{-}ESMADKT}$ −2.0	−288.3
			$\upsilon_{M}^{ETAM\text{-}EDTAM}$ 1.57	$\upsilon_{Cr}^{ESMAD\text{-}ESMADKT}$ 2.89	165.2
			$\upsilon_{D}^{ETAM\text{-}EDTAM}$ −118.49	$\upsilon_{Fe}^{ESMAD\text{-}ESMADKT}$ 4.94	−334.1
				$\upsilon_{E}^{ESMAD\text{-}ESMADKT}$ 7.95	2772.0
				$\upsilon_{S}^{ESMAD\text{-}ESMADKT}$ −1.80	−102.5
				$\upsilon_{M}^{ESMAD\text{-}ESMADKT}$ 1.03	146.2
				$\upsilon_{A}^{ESMAD\text{-}ESMADKT}$ 0.39	340.1
				$\upsilon_{D}^{ESMAD\text{-}ESMADKT}$ −8.40	−961.0
				$\upsilon_{K}^{ESMAD\text{-}ESMADKT}$ −4.94	−350.8
				$\upsilon_{I}^{ESMAD\text{-}ESMADKT}$ −12.34	−2503.2

	5-Component Model			7-Component Model	
	Case 1	Case 2	Case 3	Case 4	Case 5
Net reaction(mol/unit-time):					
υ_{F}	−86.93	−63.34	−231.67	−17.83	−3360.0
υ_{E}	152.93	126.37	439.34	40.02	7393.5
υ_{S}	10.46	0.16	12	1.89	175.8
υ_{M}	0	0	0	1.03	147.1
υ_{A}	−10.46	−0.16	−12	−0.38	−35.2
υ_{D}	20.93	0.31	24	−9.09	−1460.0
υ_{K}	–	–	–	−4.94	−350.8
υ_{I}	−66	−63.03	−207.67	−12.34	−2503.2
υ_{P}	0	0	0	−2	−290
υ_{Cr}	–	–	–	−3	−280
υ_{Fe}	–	–	–	5	550
υ_{O2}†	–	–	–	−2.52	−188.8

Case 1: F | ESM | EAM | EDAM | EDTAM.
Case 2: F | ESM | EAM | EDAM | EDTAM.
Case 3: F | ES | EM | EDM | EAM | ETAM | EDTAM.
Case 4: F | ES | ESM | ESMA | ESMAD | ESMADKT.
Case 5: F | ES | ESM | ESMA | ESMAD | ESMADKT.

* Arbitrarily specified.

** Matrix modes for cases 1–3 are identical except for variable M.

† Calculated from the net reaction coefficients υ_P, υ_{Cr}, υ_{Fe} by assuming that metal was the open-system source for P and Cr and the sink for Fe, and consequently that the net reaction coefficients υ_P, υ_{Cr}, υ_{Fe} refer to metallic components.

model, the net reaction for any set of L-ratios is a combination of the two following principal reactions:

$$\underset{\text{forsterite}}{Mg_2SiO_4} + \underset{\text{tridymite}}{SiO_2} = \underset{\text{enstatite}}{2MgSiO_3} \quad [1]$$

$$\underset{\text{forsterite}}{2Mg_2SiO_4} + \underset{\text{anorthite}}{CaAl_2Si_2O_8} = \underset{\text{enstatite}}{2MgSiO_3} + \underset{\text{diopside}}{2Mg_{0.5}Ca_{0.5}SiO_3} + \underset{\text{spinel}}{MgAl_2O_4} \quad [2]$$

Model results suggest that ≈15 to 35 times as much orthopyroxene was produced by reaction [1] as by reaction [2] for Emery coronas, and that ≈55 times as much orthopyroxene was produced by reaction [1] as by reaction [2] for Morristown coronas.

The 5-component model has difficulty in simultaneously accounting for three features of the coronas in Emery and Morristown (table 1), including: (1) the low abundance (≤5 vol percent) of clinopyroxene in the outer zone, (2) the high abundance of merrillite in the middle (>10 vol percent) and outer zones (>5 vol percent) of Emery coronas, and (3) the relatively thick inner zones (≈15-25% of total corona width) of Emery coronas. In general, the discrepancies between the actual and 5-component model coronas are worse for Emery. An additional *net* reaction involving the removal of clinopyroxene and the formation of merrillite appears to be required for Emery and perhaps for Morristown to account for these discrepancies. Such an additional net reaction is obtained in the 7-component models (see below).

7-Component Model Coronas—Two Examples

Model results for two 7-component coronas with the zone sequence F|ES|ESM|ESMA|ESMAD|ESMADKT are shown in figure 3 and table 3. Calculations for the 7-component model show that the value of the diffusivity parameter L_{SiSi} and the magnitude of open-system fluxes have large effects on layer growth. For the L_{SiSi}-high case (fig. 3A; table 3, case 4), an attempt was made to maximize the value of L_{SiSi} relative to other L-coefficients while still obtaining a model corona that resembles coronas in Emery. For the L_{SiSi}-low case (fig. 3B; table 3, case 5), an attempt was made to minimize the value of L_{SiSi} relative to other L-coefficients while still obtaining a model corona that resembles coronas in Emery.

In both model coronas, a flux of Fe out of the coronas at the ESMAD-ESMADKT contact ($J_{Fe}^{out} > 0$) and a flux of P and Cr into the coronas at the ESMAD-ESMADKT contact ($J_P^{out} < 0$ and $J_{Cr}^{out} < 0$, or equivalently $J_P^{in} > 0$ and $J_{Cr}^{in} > 0$) is required. An open-system influx of P and Cr into the coronas is required to explain the high abundances of merrillite and chromite within coronas. An open-system outflow of Fe is required to explain the depletion of metal in coronas relative to matrix.

For both model coronas, μ_{MgO} and μ_{FeO} decrease while μ_{SiO_2} and $\mu_{CrO_{3/2}}$ increase from F to ESMADKT, and $\mu_{AlO_{3/2}}$ has a local maximum at the ESM-ESMA contact (fig. 3A, B). This implies that MgO and FeO are diffusing away from olivine, that SiO_2 and $CrO_{3/2}$ are diffusing away from matrix, and that $AlO_{3/2}$ is diffusing away from the ESM-ESMA contact.

A relatively high value of L_{SiSi} will minimize the change of μ_{SiO_2} relative to the change of μ_i for other components (fig. 3A) and will minimize the values of reaction coefficients of all components relative to Si (table 3, case 4). To account for the observations with a high value of L_{SiSi}, open-system outflows of Fe and inflows of Cr and P at the corona-matrix contact are required to be small (but non-zero) relative to the rate at which SiO_2 evolved at this contact (fig. 3A), and L_{FeFe}, L_{MgMg}, L_{AlAl}, and especially L_{PP} are required to be small. The value of L_{CrCr} can be larger, about as large as L_{SiSi}. An extremely low value for L_{PP} means that $PO_{5/2}$ will diffuse very sluggishly, and thus P-bearing merrillite (M) will be concentrated in zones where $\mu_{PO_{5/2}}$ is high, in this case a narrow ESM zone (fig. 3A). In contrast, the moderate value of L_{CrCr} allows $CrO_{3/2}$ to be

effectively transported away from the ESMADKT reactant (where $\mu_{CrO_{3/2}}$ is high) to form abundant chromite (S) in relatively distant zones where $\mu_{CrO_{3/2}}$ is low, in this case two thin ES and ESM zones (fig. 3A).

On the other hand, a relatively low value of L_{SiSi} will maximize the change of μ_{SiO_2} relative to the change of μ_i for other components (fig. 3B) and will maximize the values of reaction coefficients for all components relative to SiO_2 (table 3, case 5). Higher reaction coefficients for FeO, $CrO_{3/2}$, and $PO_{5/2}$ require a larger open-system outflow of Fe and inflow of Cr and P relative to rate at which SiO_2 is evolved at the corona-matrix contact (fig. 3B; table 3, case 5). Higher diffusivities of $AlO_{3/2}$, CaO, and $PO_{5/2}$ relative to SiO_2 cause these components to be more rapidly transported away from areas where they have high values of chemical potential, resulting in gradational variations in $\mu_{AlO_{3/2}}$, μ_{CaO}, and $\mu_{PO_{5/2}}$ (fig. 3B). This results in a more uniform distribution of Al-bearing chromite (S) and merrillite (M) throughout this model corona (fig. 3B) than in the previous one (fig. 3A).

7-Component Model–Correspondence to Actual Coronas

With the 7-component model, the model sequence F|ES|ESM|ESMA|ESMAD|ESMADKT provides the best analog to coronas in Emery. The ES, ESMA, and ESMAD zones in the model coronas appear to correspond to the inner, middle, and outer zones of Emery coronas, respectively (compare table 1A and fig. 3A). The ESM zone, which is rich in merrillite, can be correlated with the inner portion of the middle zone of Emery coronas, which is usually merrillite-rich and sometimes depleted in plagioclase compared to the rest of the middle zone. A chromite necklace is often present at the inner-middle zone contact in Emery coronas (Delaney and others, 1981; Ruzicka and others, 1994), and this may correspond to the thin, chromite (S)-rich portion of the ES zone produced in L_{SiSi}-high model coronas (fig. 3A).

Buffering by Fe-bearing orthopyroxene causes FeO to diffuse away from olivine to matrix (fig. 3), and this will tend to produce Fe-rich phases (especially metal) close to the matrix. An open-system flux of Fe out of the coronas and into matrix (J_{Fe}^{out}) must be established and be of a sufficient magnitude to destabilize metal and form the metal-poor olivine coronas that are observed in mesosiderites. Moreover, an open-system flux of Cr and P into the coronas from matrix (J_{Cr}^{in}, J_P^{in}) is needed to account for the relatively high abundance of chromite and merrillite in coronas and for the distribution of these phases in the coronas. The best matches to Emery coronas are obtained when $J_{Cr}^{in} \approx J_P^{in} \approx 0.5 \cdot J_{Fe}^{out}$, suggesting that *the flux of material entering the coronas was approximately the same as the flux leaving the coronas.*

Unlike the 5-component model, the 7-component model has little difficulty in accounting for the low abundance of clinopyroxene in the outer zone of coronas, although the merrillite contents are still somewhat low (compare fig. 3 and table 1A). An open-system flux of $PO_{5/2}$ into coronas from the matrix, combined with a low value of L_{PP}, stabilizes merrillite in the outer zone. As more merrillite forms in this zone, more Ca goes to form merrillite, and less is available to form clinopyroxene. Consequently, less clinopyroxene forms in the outer zone. This inverse relationship between the abundance of merrillite and clinopyroxene in the outer zone is more pronounced in the 7-component model, where the amount of Ca in matrix is fixed, than in the 5-component model, where the amount of P and Ca in matrix covary depending on the amount of merrillite that is assumed to be present in matrix. These results suggest that *much (or all) of the P that went to form corona merrillite in mesosiderites was derived from a phase other than merrillite.*

The values of L-coefficient ratios most appropriate to corona growth in mesosiderites are difficult to constrain uniquely with the 7-component model, owing to the

uncertainty in the values for open-system fluxes. In the models, all open-system fluxes were scaled relative to an arbitrary value of $\upsilon_S^{\text{ESMAD-ESMADKT}} = 12$ moles/[unit time]. As discussed below, a large variation in acceptable values of relative L-coefficients, especially in relative L_{SiSi}, are possible depending on the magnitude of the open-system fluxes of Fe, P, and Cr.

For *small values of open-system outflow and inflow,* L_{SiSi} must be relatively large (corresponding to the L_{SiSi}-high case, fig. 3A), and $L_{SiSi} \geq L_{CrCr} \geq L_{MgMg} \geq L_{FeFe} \approx L_{AlAl} \approx L_{CaCa} > L_{PP}$, where $L_{SiSi} \approx 1000\ L_{PP}$, $J_{Cr}^{in}, J_{P}^{in} \approx 2$ to 3 mol/[unit area-time], and $J_{Fe}^{out} \approx 5$ mol/[unit area-time]. For *intermediate values of open-system outflow and inflow,* $L_{MgMg} \approx L_{CrCr} \approx L_{FeFe} \approx L_{SiSi} > L_{AlAl} > L_{CaCa} > L_{PP}$, where $L_{SiSi} \approx 100\ L_{PP}$. Finally, for *large values of open-system outflow and inflow,* L_{SiSi} must be relatively small (corresponding to the L_{SiSi}-low case, fig. 3B), and $L_{MgMg} \geq L_{FeFe} \geq L_{AlAl} \approx L_{CrCr} > L_{CaCa} > L_{SiSi} > L_{PP}$, where $L_{SiSi} \approx 0.01\ L_{MgMg} \approx 0.02\ L_{CrCr} \approx 10\ L_{PP}$, $J_{Cr}^{in} \approx J_{P}^{in} \approx 280$ to 290 mol/[unit area-time], and $J_{Fe}^{out} \approx 550$ mol/[unit area-time].

Inferences concerning L-ratios based on the 7-component model when small values of open-system fluxes are assumed are consistent with inferences based on the 5-component model when open-system fluxes are neglected (see above). This suggests that despite differences in phase compositions and matrix modes, the two types of models yield consistent results.

The difficulty in obtaining unique constraints on L-ratios is an important result of the 7-component model, for it shows that *inferring unique values of L-ratios for a layering structure may be difficult if open-system fluxes are present.* This agrees with the conclusions of Johnson and Carlson (1990) and Carlson and Johnson (1991). These authors also argued that open-system fluxes are often involved in the formation of coronas.

An estimate of the net corona-forming reaction for Emery can be obtained by assuming that the L_{SiSi}-high and L_{SiSi}-low cases bracket the likely conditions for corona growth in Emery. Normalizing the net reaction coefficients for these cases (table 3, cases 4-5) to 1 mole of tridymite, the net corona-forming reaction may be expressed as:

$$\underset{\text{olivine}}{1.34\text{–}1.44\ F} + \underset{\text{plagioclase}}{0.01\text{–}0.03\ A} + \underset{\text{clinopyroxene}}{0.58\text{–}0.74\ D} + \underset{\text{metal}}{0.14\text{–}0.40\ K}$$
$$+ \underset{\text{tridymite}}{1.00\ T} + \underset{\text{open-system}}{0.11\text{–}0.24\ Cr_2O_3} + \underset{\text{open-system}}{0.12\text{–}0.16\ P_2O_5}$$
$$\rightarrow \underset{\text{orthopyroxene}}{2.95\text{–}3.24\ E} + \underset{\text{chromite}}{0.07\text{–}0.15\ S} + \underset{\text{merrillite}}{0.06\text{–}0.08\ M} + \underset{\text{open-system}}{0.22\text{–}0.41\ FeO} \quad [3]$$

where phase compositions are given in table 2 ("7-component model"), and the first value for each entry refers to the L_{SiSi}-low case, and the second value for each entry refers to the L_{SiSi}-high case. In reaction [3], Cr_2O_3 and P_2O_5 are reactants and FeO is a product because of the assumed open-system fluxes of Cr and P into coronas and of Fe out of the coronas. These open-system fluxes are responsible for the overall production of chromite and merrillite and for the removal of metal in the coronas. Anorthite is a net reactant because the production of Al-bearing chromite requires $AlO_{3/2}$ to be removed from another phase, and anorthite is the only other Al-bearing phase in the system. Clinopyroxene is a net reactant because the production of merrillite requires Ca to be removed from other phases, and Ca-rich clinopyroxene is available for this purpose. Abundant orthopyroxene is produced mainly because this phase is intermediate in composition between the two main reacting phases, tridymite and olivine.

As discussed by Ruzicka and others (1994), the "excess" P and Cr in coronas (see Introduction) was probably derived from a large volume of matrix metal, and matrix metal could also have been the ultimate sink for the Fe that diffused out of coronas.

Assuming that metal was the "open-system" source and sink reservoir for P, Cr, and Fe, reaction [3] may be recast as:

$$\underset{\text{olivine}}{1.34\text{–}1.44\ F} + \underset{\text{plagioclase}}{0.01\text{–}0.03\ A} + \underset{\text{clinopyroxene}}{0.58\text{–}0.74\ D} + \underset{\text{metal}}{0.14\text{–}0.40\ K}$$
$$+ \underset{\text{tridymite}}{1.00\ T} + \underset{\text{open-system}}{0.11\text{–}0.24\ Cr^\circ} + \underset{\text{open-system}}{0.12\text{–}0.16\ P^\circ} + \underset{\text{open-system}}{0.08\text{–}0.20\ O_2}$$
$$\rightarrow \underset{\text{orthopyroxene}}{2.95\text{–}3.24\ E} + \underset{\text{chromite}}{0.07\text{–}0.15\ S} + \underset{\text{merrillite}}{0.06\text{–}0.08\ M} + \underset{\text{open-system}}{0.22\text{–}0.41\ Fe^\circ} \quad [4]$$

where O_2 could have been supplied by redox reactions in mesosiderites occurring outside of coronas (Harlow and others, 1982; Ruzicka and others, 1994, p. 2738-2739). In reaction [4], a distinction is made between metal that was removed from the corona-forming region (designated as "K") and open-system metallic components that presumably resided in a much larger volume of matrix metal. If the identification of metal as the open-system reservoir for P, Cr, and Fe is correct, then reaction [4] implies that the amount of Fe-rich metal removed from the corona-forming region (K) was similar to the amount of Fe-metal produced in the adjacent matrix (Fe°). In other words, *metal was largely transferred from the corona-forming region to the adjacent matrix.* Reaction [4] also suggests that the large reservoir of "open-system" matrix metal changed composition, becoming poorer in Cr and P and richer in Fe with time. This implies that *in the large reservoir of matrix surrounding coronas, Cr and P were oxidized, and FeO was reduced.* Reduction of FeO within a large volume of the mesosiderites is consistent with evidence for the reduction of FeO in basalt/gabbro clasts in these meteorites (Mittlefehldt, 1990) and is cosistent with thermodynamic predictions for mesosiderites (Harlow and others, 1982). Reduction of FeO in a large volume of the mesosiderites apparently occurred despite evidence that metallic Fe *within* coronas was oxidized (Ruzicka and others, 1994).

CONCLUSIONS

Mineral zone structures such as coronas provide a unique opportunity to unravel the nature and kinetics of diffusion and reaction processes that occurred during metamorphism. The Fisher-Joesten steady-state growth model for mineral zone structures has been refined, and the residual-concentration-effect has been formalized and incorporated into equations for layer growth, allowing polymineralic reactants to be readily modelled in addition to monomineralic reactants. The equations also easily accommodate various diffusion geometries (for example, planar or concentric) and either open- or closed-system diffusion.

As shown by an application of the theory to olivine coronas in mesosiderites, if one or both of the original reactants are polymineralic, then it is possible for a mineral that is removed by an overall structure-forming reaction to be stable within one or more zones within the structure and for a mineral to disappear from one part of the structure and to reappear in another part. In the general case, it may be difficult to tightly constrain the ratios of Onsager diffusion (L-) coefficients if open-system fluxes are known or suspected to have occurred; conversely, it may be difficult to tightly constrain the magnitude of open-system fluxes if the Onsager diffusion coefficients are poorly known. Nonetheless, the models do permit some useful constraints to be obtained on the L-ratios, open-system fluxes, and local and overall reactions responsible for layer growth processes during metamorphism.

The textures and compositions of olivine coronas in the Emery and Morristown mesosiderites can be successfully modelled as having formed by a quasi-steady-state, coupled reaction-diffusion process. In Emery, it appears that P and Cr diffused into the coronas from matrix and that Fe diffused out of the coronas into matrix, during open-system diffusion. A phase other than merrillite, probably P-bearing metal, was the

source of P that ultimately was transported to coronas to form merrillite. The open-system flux of material leaving the coronas was about the same as the open-system flux of material entering the coronas. The cumulative effect of local reactions within coronas in Emery was to remove olivine, tridymite, plagioclase, metal, and clinopyroxene, and to produce orthopyroxene, chromite, and merrillite. It seems likely that metal was largely transferred by diffusional processes from the corona-forming region to the adjacent matrix, and that oxygen was supplied to the coronas from the surrounding matrix.

ACKNOWLEDGMENTS

The author wishes to thank Ray Joesten, Tom Foster, Bill Carlson, George Harlow, and Sumit Chakraborty for constructive (and thorough) reviews of various iterations of this manuscript and Melinda Hutson for her valued assistance. This work was supported by NASA grant NAG 9-460 to W. V. Boynton.

REFERENCES

Ashworth, J. R., and Birdi, J. J., 1990. Diffusion modelling of coronas around olivine in an open system: Geochimica et Cosmochimica Acta, v. 54, p. 2389–2401.

Ashworth, J. R., Birdi, J. J., and Emmett, T. F., 1992, Diffusion in coronas around clinopyroxene–modelling with local equilibrium and steady state, and a non-steady state modification to account for zoned actinolite-hornblende: Contributions to Mineralogy and Petrology, v. 109, p. 307–325.

Brady, J. B., 1975, Reference frames and diffusion coefficients: American Journal of Science, v. 275, p. 954–983.

——— 1977, Metasomatic zones in metamorphic rocks: Geochimica et Cosmochimica Acta, v. 41, p. 113–125.

Carlson, W. D., and Johnson, C. D., 1991, Coronal reaction textures in garnet amphibolites of the Llano Uplift: American Mineralogist, v. 76, p. 756–772.

Delaney, J. S., Nehru, C. E., Prinz, M., and Harlow, G. E., 1981, Metamorphism in mesosiderites, *in* Proceedings of the Twelfth Lunar and Planetary Science Conference, Geochimica et Cosmochimica Acta Suppl., v. 12, p. 1315–1342.

Fisher, G. W., 1973, Nonequilibrium thermodynamics as a model for diffusion-controlled metamorphic processes: American Journal of Science, v. 272, p. 897–924.

——— 1977, Nonequilibrium thermodynamics in metamorphism, *in* Fraser, D. G., editor, Thermodynamics in Geology: Dordrecht-Holland, D. Reidel, p. 381–403.

——— 1978, Rate laws in metamorphism: Geochimica et Cosmochimica Acta, v. 42, p. 1035–1050.

Fisher, G. W., and Elliot, D., 1974, Criteria for quasi-steady diffusion and local equilibrium in metamorphism, *in* Hofmann, A. W., Giletti, B. J., Yoder, H. S. Jr., and Yund, R. A., editors, Geochemical Transport and Kinetics: Carnegie Institute of Washington, Publication 634, p. 231–241.

Fisher, G. W., and Lasaga, A. C., 1981, Irreversible thermodynamics in petrology, *in* Lasaga, A. C., and Kirkpatrick, R. J., editors, Kinetics of Geochemical Processes, Reviews in Mineralogy, v. 8: Mineralogical Society of America.

Floran, R. J., 1978, Silicate petrography, classification, and origin of the mesosiderites–Review and new observations, *in* Proceedings of the Ninth Lunar and Planetary Science Conference, Geochimica et Cosmochimica Acta Supplement, v. 9, p. 1053–1081.

Foster, C. T., Jr., 1981, A thermodynamic model of mineral segregations in the lower sillimanite zone near Rangely, Maine: American Mineralogist, v. 66, p. 260–277.

——— 1983, Thermodynamic models of biotite pseudomorphs after staurolite: American Mineralogist, v. 68, p. 389–397.

——— 1986, Thermodynamic models of reactions involving garnet in a sillimanite/staurolite schist: Mineralogical Magazine, v. 50, p. 427–439.

——— 1991, The role of biotite as a catalyst in reaction mechanisms that form sillimanite: Canadian Mineralogist, v. 29, p. 943–963.

Frantz, J. D., and Mao, H. K., 1975, Metasomatism and metamorphism: Carnegie Institute of Washington Year Book, v. 74, p. 417–428.

——— 1976, Bimetasomatism resulting from intergranular diffusion–I. A theoretical model for monomeralic reaction zone sequences: American Journal of Science, v. 276, p. 817–840.

——— 1979, Bimetasomatism resulting from intergranular diffusion–II. Prediction of multimineralic zone sequences: American Journal of Science, v. 279, p. 302–323.

Harlow, G. E., Delaney, J. S., Nehru, C. E., and Prinz, M., 1982, Metamorphic reactions in mesosiderites–origin of abundant phosphate and silica: Geochimica et Cosmochimica Acta v. 46, p. 339–348.

Hartley, G. S., and Crank, J., 1949, Some fundamental definitions and concepts in diffusion processes: Transactions of the Faraday Society, v. 45, p. 801–818.

Joesten, R., 1977, Evolution of mineral assemblage zoning in diffusion metasomatism: Geochimica et Cosmochimica Acta, v. 41, p. 649–670.

——— 1986a, The role of magmatic reaction, diffusion and annealing in the evolution of coronitic microstructure in troctolitic gabbro from Risör, Norway: Mineralogical Magazine, v. 50, p. 441–467.

——— 1986b, Reply: Mineralogical Magazine, v. 50, p. 474–479.

——— 1991, Local equilibrium in metasomatic processes revisited: Diffusion-controlled growth of chert nodule reaction rims in dolomite: American Mineralogist, v. 76, p. 743–755.

Johnson, C. D., and Carlson, W. D., 1990, The origin of olivine-plagioclase coronas in metagabbros from the Adirondack Mountains, New York: Journal of Metamorphic Geology, v. 8, p. 697–717.

Katchalsky, A., and Curran, P. F., 1965, Nonequilibrium Thermodynamics in Biophysics: Cambridge, Massachusettes, Harvard University Press, 248 p.

Korzhinskii, D. S., 1959, Physiochemical basis of the analysis of the paragenesis of minerals: Consultants Bureau, 142 p.

——— 1971, Theory of metasomatic zoning: Oxford University Press, 162 p.

Mittlefehldt, D. W., 1990, Petrogenesis of mesosiderites–I. Origin of mafic lithologies and comparison with basaltic achondrites: Geochimica et Cosmochimica Acta, v. 54, p. 1165–1173.

Nehru, C. E., Zucker, S. M., Harlow, G. E., and Prinz, M., 1980, Olivines and olivine coronas in mesosiderites: Geochimica et Cosmochimica Acta, v. 44, p. 1103–1118.

Powell, B. N., 1971, Petrology and chemistry of mesosiderites–II. Silicate textures and compositions and metal-silicate relationships, Geochimica et Cosmochimica Acta, v. 35, p. 5–34.

Ruzicka, A., ms, Ph.D. dissertation, 1996, Petrologic-kinetic studies of meteorites: Lunar and Planetary Laboratory, Department of Planetary Sciences, University of Arizona, Tucson, Arizona, 300 p.

Ruzicka, A., Boynton, W. V., and Ganguly, J., 1994, Olivine coronas, metamorphism, and the thermal history of the Morristown and Emery mesosiderites: Geochimica et Cosmochimica Acta, v. 58, p. 2725–2741.

Swapp, S. M., 1988, Mass transfer and coupled reactions in low grade metamorphism of calcareous concretions: American Journal of Science, v. 286, p. 433–462.

Thompson, J. B., Jr., 1959, Local equilibrium in metasomatic processes, in Abelson, P. H., ed. Researches in Geochemistry, v. 1: New York, John Wiley & Sons, p. 427–457.

Weare, J. H., Stevens, J. R., and Eugster, H. P., 1976, Diffusion metasomatism and mineral reaction zones–General principles and application to feldspar alteration: American Journal of Science, v. 276, p. 767–816.